Supplementary Information

Supplementary Tables

Supplemental Table S1. Strains and plasmids

Strain	Description	Reference
Sinorhizobium meliloti		
Rm1021	Wildtype *S. meliloti* Derived from SU47 (Isolated in Australia), Sm^R	**Maeder et al. 1982 (1)**
Rm5000	Wildtype *S. meliloti* Derived from SU47 (Isolated in Australia), Rf^R	**Finan et al. 1984 (2)**
RmP110	Wildtype *S. meliloti* Derived from Rm1021 with Corrected *pstC* Allele	**Yuan et al. 2006 (3)**
RmP4330	Natural *S. meliloti* Strain HM006 (Isolated in France)	**Nelson et al. 2018 (4)**
T073	Natural *S. meliloti* Strain T073 (Isolated in Tunesia)	**Nelson et al. 2018 (4)**
KH46C	Natural *S. meliloti* Strain KH46C (Isolated in France)	**Nelson et al. 2018 (4)**
USDA1106	Natural *S. meliloti* Strain USDA1106 (Isolated in California), USA	**Nelson et al. 2018 (4)**
WSM419	Wildtype *S. medicae* (Isolated in Italy), Cm^R	**Reeve et al. 2010 (5)**
RmP4246	Rm5000 ΔpSymA, Rf^R	**Sather et al. 2023 (6)**
RmP4247	RmP110 ΔpSymA, Sm^R	**Geddes et al. 2021 (7)**
RmP4275	Rm5000 ΔpSymAB, Rf^R Sp^R	**This Work**
RmP4355	WSM419 with pTH3275 Integrated by Homologous Recombination, Cm^R Gm^R	**This Work**
RmP4451	WSM419 with pTH3331 Integrated by Homologous Recombination, Cm^R Nm^R	**This Work**
RmP4393	RmP4246 with WSM419 pSymA, Rf^R Gm^R	**This Work**
RmP4410	RmP4246 with RmP110 pSymA, Rf^R	**This Work**
RmP4411	RmP4246 with USDA1106 pSymA, Rf^R	**This Work**
RmP4412	RmP4246 with HM006 pSymA, Rf^R	**This Work**
RmP4414	RmP4246 with T073 pSymA, Rf^R	**This Work**
RmP4417	RmP4246 with KH46 pSymA, Rf^R	**This Work**
RmP4452	RmP4275 with WSM419 pSymAB, Rf^R Sp^R Gm^R Nm^R	**This Work**
RmP4453	RmP4275 with WSM419 pSymB and Rmp110 pSymA, Rf^R Sp^R Nm^R	**This Work**
RmP4459	RmP4275 with HM006 pSymB and RmP110 pSymA, Rf^R Sp^R	**This Work**
RmP4460	RmP4275 with HM006 pSymAB, Rf^R Sp^R	**This Work**
RmP4463	RmP4275 with T073 pSymB and RmP110 pSymA, Rf^R Sp^R	**This Work**
RmP4464	RmP4275 with T073 pSymAB, Rf^R Sp^R	**This Work**
RmP4465	RmP4275 with USDA1106 pSymB and RmP110 pSymA, Rf^R Sp^R	**This Work**
RmP4466	RmP4275 with USDA1106 pSymAB, Rf^R Sp^R	**This Work**
RmP4467	RmP4275 with KH46 pSymB and RmP110 pSymA, Rf^R Sp^R	**This Work**
RmP4468	RmP4275 with KH46 pSymAB, Rf^R Sp^R	**This Work**
RmP4469	RmP4275 with RmP110 pSymAB, Rf^R Sp^R	**This Work**
RmP4566	RmP4247 with HM006 pSymA	**This Work**
RmND063	RmP4566, Deletion 1 (HM006 pSymA nt 511,957 – 735,761) via RmND055 with pTH1944 FLP; Sm^R Nm^R Tc^R	**This Work**
RmND064	RmP4566, Deletion 2 (HM006 pSymA nt 1,174,284 – 1,366,930) via RmND056 with pTH1944 FLP; Sm^R Nm^R Tc^R	**This Work**
RmND065	RmP4566, Deletion 3 (HM006 pSymA nt 511,957 – 540,044) via RmND057 with pTH1944 FLP; Sm^R Nm^R Tc^R	**This Work**
RmND101	RmP4566, Deletion 4 (HM006 pSymA nt 541,059 – 549,072) via RmND093 with pTH1944 FLP; Sm^R Gm^R Tc^R	**This Work**
RmND102	RmP4566, Deletion 5 (HM006 pSymA nt 549,895 – 561,440) via RmND094 with pTH1944 FLP; Sm^R Nm^R Tc^R	**This Work**
RmND103	RmP4566, Deletion 6 (HM006 pSymA nt 562,112 – 580,734) via RmND095 with pTH1944 FLP; Sm^R Gm^R Tc^R	**This Work**

RmND104	RmP4566, Deletion 7 (HM006 pSymA nt 581,374 – 641,748) via RmND096 with pTH1944 FLP; Sm^R Nm^R Tc^R	**This Work**
RmND105	RmP4566, Deletion 8 (HM006 pSymA nt 642,321 – 659,345) via RmND097 with pTH1944 FLP; Sm^R Gm^R Tc^R	**This Work**
RmND106	RmP4566, Deletion 9 (HM006 pSymA nt 660,573 – 695,749) via RmND098 with pTH1944 FLP; Sm^R Nm^R Tc^R	**This Work**
RmND107	RmP4566, Deletion 10 (HM006 pSymA nt 696,290 – 719,139) via RmND099 with pTH1944 FLP; Sm^R Gm^R Tc^R	**This Work**
RmND108	RmP4566, Deletion 11 (HM006 pSymA nt 719,869 – 735,761) via RmND100 with pTH1944 FLP; Sm^R Nm^R Tc^R	**This Work**
RmND199	RmP4566, Deletion 14 (HM006 pSymA nt 603,905 – 621,607) via RmND183 with pTH1944 FLP; Sm^R Nm^R Tc^R	**This Work**
RmND200	RmP4566, Deletion 15 (HM006 pSymA nt 623,429 – 634,973) via RmND184 with pTH1944 FLP; Sm^R Gm^R Tc^R	**This Work**
RmND201	RmP4566, Deletion 16 (HM006 pSymA nt 635,364 – 641,748) via RmND185 with pTH1944 FLP; Sm^R Nm^R Tc^R	**This Work**
RmND340	RmP4566, Deletion 17 (HM006 pSymA nt 660,573 – 679,738) via RmND321 with pTH1944 FLP; Sm^R Nm^R Tc^R	**This Work**
RmND365	RmP4566, Deletion 18 (HM006 pSymA nt 680,028 – 685,775) via RmND342 with pTH1944 FLP; Sm^R Gm^R Tc^R	**This Work**
RmND337	RmP4566, Deletion 19 (HM006 pSymA nt 686,200 – 695,749) via RmND327 with pTH1944 FLP; Sm^R Nm^R Tc^R	**This Work**
RmND055	RmND053 with pNDMS020 Integrated; Sm^R Nm^R Gm^R	**This Work**
RmND056	RmND054 with pNDMS022 Integrated; Sm^R Nm^R Gm^R	**This Work**
RmND057	RmND053 with pNDMS021 Integrated; Sm^R Nm^R Gm^R	**This Work**
RmND093	RmND088 with pNDMS028 Integrated; Sm^R Nm^R Gm^R	**This Work**
RmND094	RmND089 with pNDMS028 Integrated; Sm^R Nm^R Gm^R	**This Work**
RmND095	RmND089 with pNDMS030 Integrated; Sm^R Nm^R Gm^R	**This Work**
RmND096	RmND090 with pNDMS030 Integrated; Sm^R Nm^R Gm^R	**This Work**
RmND097	RmND090 with pNDMS032 Integrated; Sm^R Nm^R Gm^R	**This Work**
RmND098	RmND091 with pNDMS032 Integrated; Sm^R Nm^R Gm^R	**This Work**
RmND099	RmND091 with pNDMS034 Integrated; Sm^R Nm^R Gm^R	**This Work**
RmND100	RmND092 with pNDMS034 Integrated; Sm^R Nm^R Gm^R	**This Work**
RmND183	RmND180 with pNDMS089 Integrated; Sm^R Nm^R Gm^R	**This Work**
RmND184	RmND180 with pNDMS091 Integrated; Sm^R Nm^R Gm^R	**This Work**
RmND185	RmND090 with pNDMS091 Integrated; Sm^R Nm^R Gm^R	**This Work**
RmND321	RmND292 with pNDMS160 Integrated; Sm^R Nm^R Gm^R	**This Work**
RmND342	RmND322 with pNDMS161 Integrated; Sm^R Nm^R Gm^R	**This Work**
RmND327	RmND091 with pNDMS161 Integrated; Sm^R Nm^R Gm^R	**This Work**
RmND053	RmP4566 with pNDMS018 Integrated; Sm^R Nm^R	**This Work**
RmND054	RmP4566 with pNDMS019 Integrated; Sm^R Nm^R	**This Work**
RmND088	RmP4566 with pNDMS021 Integrated; Sm^R Gm^R	**This Work**
RmND089	RmP4566 with pNDMS029 Integrated; Sm^R Gm^R	**This Work**
RmND090	RmP4566 with pNDMS031 Integrated; Sm^R Gm^R	**This Work**
RmND091	RmP4566 with pNDMS033 Integrated; Sm^R Gm^R	**This Work**
RmND092	RmP4566 with pNDMS020 Integrated; Sm^R Gm^R	**This Work**
RmND180	RmP4566 with pNDMS090 Integrated; Sm^R Gm^R	**This Work**
RmND292	RmP4566 with pNDMS032 Integrated; Sm^R Nm^R	**This Work**
RmND322	RmP4566 with pNDMD160 Integrated; Sm^R Gm^R	**This Work**
RmND393	RmP4566 with pNDMS193 (pPha) Introduced; Sm^R Tc^R	**This Work**
RmND488	RmP4566 with pNDMS242 (pNodA) Introduced; Sm^R Tc^R	**This Work**
RmND489	RmP4566 with pNDMS211 (pNifH) Introduced; Sm^R Tc^R	**This Work**
RmND219	Φ RmND190 (*ctrl-1*) → RmP110; Sm^R Sp^R	**This Work**
RmND220	Φ RmND191 (*pha-1*) → RmP110; Sm^R Sp^R	**This Work**
RmND221	Φ RmND192 (*ctrl-2*) → RmP110; Sm^R Sp^R	**This Work**
RmND522	Φ RmND468 (*att*) → RmND220; Sm^R Sp^R Nm^R	**This Work**
RmND190	RmP4657 with pNDMS119 Integrated via FLP/FRT; Sm^R Sp^R Tc^R	**This Work**
RmND191	RmP4657 with pNDMS120 Integrated via FLP/FRT; Sm^R Sp^R Tc^R	**This Work**
RmND192	RmP4657 with pNDMS121 Integrated via FLP/FRT; Sm^R Sp^R Tc^R	**This Work**
RmND468	RmP4253 with pNDMS041 Integrated via FLP/FRT; Sm^R Nm^R Tc^R	**This Work**

RmP4657	Landing Pad Including *FRT* Site Based in *manB* and a Protocatechuate Inducible Flippase (pTH2505); Sm^R Tc^R	**Geddes et al. 2021 (7)**
RmND548	RmP4566 with pNDMS250 Integrated (*ghbD^{pha-1}::Nm)*; Sm^R Nm^R	**This Work**
RmND652	RmP4566 with pNDMS303 Integrated (*ghbD^{pha-2}::Gm)*; Sm^R Gm^R	**This Work**
RmND653	RmND548 with pNDMS303 Integrated (*ghbD^{pha-1}::Nm* & *ghbD^{pha-2}::Gm)*; Sm^R Nm^R Gm^R	**This Work**
RmND329	RmP4566 with pNDMS078 Integrated (*phaC2^{pha-1}::Nm)*; Sm^R Nm^R	**This Work**
RmND287	RmP4566 with pNDMS073 Integrated (*phaC2^{pha-2}::Gm)*; Sm^R Gm^R	**This Work**
RmND330	RmND287 with pNDMS078 Integrated (*phaC2^{pha-1}::Nm* & *phaC2^{pha-2}::Gm*); Sm^R Nm^R Gm^R	**This Work**
RmND550	RmP4566 with pNDMS252 Integrated (*ghbT::Gm)*; Sm^R Gm^R	**This Work**
RmND549	RmP4566 with pNDMS251 Integrated (*acs::Nm)*; Sm^R Nm^R	**This Work**
RmND949	RmND256 with pNDMS250 Integrated (*ghbD^{pha-1}::Nm)*; Sm^R Nm^R	**This Work**
RmND952	RmND256 with pNDMS303 Integrated (*ghbD^{pha-1}::Nm* & *ghbD^{pha-2}::Gm*); Sm^R Nm^R Gm^R	**This Work**
RmND256	RmP4330 (Wildtype HM006) with Gained Sm^R	**This Work**
RmND866	Φ RmND847 (*ghbD*) → RmP110; Sm^R Sp^R	**This Work**
RmND867	Φ RmND848 (*ghbD* & *attL*) → RmP110; Sm^R Sp^R	**This Work**
RmND847	RmP4657 with pNDMS514 Integrated via FLP/FRT; Sm^R Sp^R Tc^R	**This Work**
RmND848	RmP4657 with pNDMS515 Integrated via FLP/FRT; Sm^R Sp^R Tc^R	**This Work**
RmP4253	Landing Pad Including *FRT* Site Based in *hypRE* and a Protocatechuate Inducible Flippase (pTH2505); Sm^R Tc^R	**Geddes et al. 2021 (7)**
Saccharomyces cerevisiae		
VL6-48	MATα his3-Δ200 trp1-Δ1 ura3−52 lys2 289 ade2−1 met14 cir	**ATCC® MYA-3666™**
Escherichia coli		
DH5-Alpha	*fhuA2Δ(argF-lacZ)U169 phoA glnV44 Φ80Δ(lacZ)M15 gyrA96 recA1 relA1 endA1 thi-1 hsdR17*	**New England BioLabs**
MT616	MM294A *recA-56* (pRK600), Mobilizer; Cm^R	**Finan et al. 1986**
Epi300	*F- mcrA* Δ(*mrr-hsdRMS-mcrBC*) *φ80dlacZΔM15* Δ*lacX74 recA1 endA1 araD139* Δ(*ara, leu*)7697 *galU galK λ- rpsL nupG trfA dhfr*; Sm^R Cm^R	**Lucigen**
M859	Rf^R DH5-Alpha	**Lab Collection**
SHuffle	*F´ lac, pro, lacI^q / Δ(ara-leu)7697 araD139 fhuA2 lacZ::T7 gene1 Δ(phoA)PvuII phoR ahpC* galE (or U) galK λatt::pNEB3-r1-cDsbC* (Spec^R, *lacI^q*) *ΔtrxB rpsL150* (Str^R) *Δgor Δ(malF)3*	**New England Biolabs**
Plasmid	**Description**	**Reference**
pNDMS331	pPGN-C with RS21600 (*ghbD*) and pICSL30015 (6xHIS-MBP-3C) via BsaI Golden Gate Cloning; Amp^R	**This Work**
pPGN-C	pOPIN-GG Expression Vector Compatible with N-Terminal Tagging (Addgene ID: 174578); Amp^R	**Bentham et al. 2021 (28)**
pICSL30015	Level 0 N-Terminal Tag Module Carrying 6xHIS-MBP-3C (Addgene ID: 174582); Sp^R	**Bentham et al. 2021 (28)**
RS21600	HM006 pSymA nt 629,955 – 631,130 (*ghbD*) Flanked by BsaI Sites for Golden Gate Cloning (Synthesized by Twist Bioscience)	**This Work**
pNDMS193	pNDGG003 (Vector) with pOPS0253 (BGND059/BGND060) (gusA), pNDGG037 (Terminator), and HM006 pSymA nt 632,983 – 633,911 (pPha using pPha F/pPha R) via BsaI Golden Gate Cloning; Tc^R	**This Work**
pNDMS242	pNDGG003 (Vector) with pOPS0253 (BGND059/BGND060) (gusA), pNDGG037 (Terminator), and pNDGG042 (pNodA) via BsaI Golden Gate Cloning; Tc^R	**This Work**
pNDMS211	pNDGG003 (Vector) with pOPS0253 (BGND059/BGND060) (gusA), pNDGG037 (Terminator), and pNDGG034 (pNifH) via BsaI Golden Gate Cloning; Tc^R	**This Work**
pTH1937	ΔTn903 Inverted Repeats, pRK2 oriT, *nptII* from Tn5, p15A *oriV*; Km^R	**Milunovic et al. 2014 (9)**
pTH3291	pTH1522 3447 bp Amplicon Including oriV/oriT, FRT Site and Gm, Circularized via BglII; Gm^R	**Geddes et al. 2021 (7)**

pTH1944	*flp* gene in a pBBR-MCS3 Derivative with RK2-tetR-tetA; Tc^R	**Milunovic et al. 2014 (9)**
pNDGG003	BEVA2.0 Broad Host Range Plasmid with Stability. L1-RK2-Tc-par-ELT4; Tc^R	**Geddes et al. 2025 (29)**
pOPS0253	Reporter Plasmid Constructed with Rlv3841 pNifH (pOGG082), gusA (pOGG083), and T-Pharma (pOGG003) Assembled in pOGG026 (Addgene ID: 115505); Nm^R	**Geddes et al. 2019 (30)**
pNDGG037	BEVA2.0 T2m Terminator for CIDAR MoClo Golden Gate Assembly; Cloned via BpiI GG Assembly of PCR Amplicon into pOGG006; Sp^R	**Geddes et al. 2025 (29)**
pNDGG042	pOGG006 with pNodA with AB extension for CIDAR MoClo Golden Gate Assembly; Sp^R	**Ardi Thesis 2023 (31)**
pNDGG034	pOGG006 with pNifH with AC extension for CIDAR MoClo Golden Gate Assembly; Sp^R	**Ardi Thesis 2023 (31)**
pNDGG014	BEVA (Gm and No FRT) P1 (pOGG004_noT) P2 (pOGG009) P3 (pTH3307 (pMBI via BsmBI)) P4 (pOGG013); Gm^R	**Geddes et al. 2025 (29)**
pNDGG015	BEVA (Km/Nm and No FRT) P1 (pOGG004_noT) P2 (pTH3309 (nptI via BsmBI)) P3 (pTH3306 (p15A via BsmBI)) P4 (pOGG013); Km^R	**Geddes et al. 2025 (29)**
FRT_EF	FRT Site for Module EF for Golden Gate Cloning via BsaI; Amp^R	**Geddes et al. 2025 (29)**
pNDMS018	pTH1937 with HM006 pSymA nt 510,905 – 511,956 (BGND001/BGND002) via KpnI/HindIII; Km^R	**This Work**
pNDMS019	pTH1937 with HM006 pSymA nt 1,173,460 – 1,174,283 (BGND005/BGND006) via KpnI/HindIII; Km^R	**This Work**
pNDMS020	pTH3291 with HM006 pSymA nt 735,762 – 736,796 (BGND003/BGND004) via BglII/PstI; Gm^R	**This Work**
pNDMS021	pTH3291 with HM006 pSymA nt 540,045 – 541,058 (BGND007/BGND008) via BglII/PstI; Gm^R	**This Work**
pNDMS022	pTH3291 with HM006 pSymA nt 1,366,931 – 1,368,079 (GLND009/GLND010) via BglII/PstI; Gm^R	**This Work**
pNDMS028	pTH1937 with HM006 pSymA nt 549,073 – 549,894 (GLND051/GLND052) via KpnI/HindIII; Km^R	**This Work**
pNDMS029	pTH3291 with HM006 pSymA nt 561,441 – 562,111 (GLND053/GLND054) via BglII/PstI; Gm^R	**This Work**
pNDMS030	pTH1937 with HM006 pSymA nt 580,735 – 581,373 (GLND055/GLND056) via KpnI/HindIII; Km^R	**This Work**
pNDMS031	pTH3291 with HM006 pSymA nt 641,749 – 642,320 (GLND057/GLND058) via BglII/PstI; Gm^R	**This Work**
pNDMS032	pTH1937 with HM006 pSymA nt 659,346 – 660,572 (GLND059/GLND060) via KpnI/HindIII; Km^R	**This Work**
pNDMS033	pTH3291 with HM006 pSymA nt 695,750 – 696,289 (GLND061/GLND062) via BglII/PstI; Gm^R	**This Work**
pNDMS034	pTH1937 with HM006 pSymA nt 719,140 – 719,868 (GLND063/GLND064) via KpnI/HindIII; Km^R	**This Work**
pNDMS089	pTH1937 with HM006 pSymA nt 602,640 – 603,904 (GLND099/GLND100) via KpnI/HindIII; Km^R	**This Work**
pNDMS090	pTH3291 with HM006 pSymA nt 621,608 – 623,428 (GLND101/GLND102 via BglII/PstI; Gm^R	**This Work**
pNDMS091	pTH1937 with HM006 pSymA nt 634,974 – 635,363 (GLND103/GLND104) via KpnI/HindIII; Km^R	**This Work**
pNDMS160	pNDGG014 with HM006 pSymA nt 679,739 – 680,027 (GLND265/GLND266) via BsaI Golden Gate Cloning; Gm^R	**This Work**
pNDMS161	pNDGG015 with HM006 pSymA nt 685,776 – 686,199 (GLND267/GLND268) via BsaI Golden Gate Cloning; Km^R	**This Work**
pNDMS119	*ctrl-1* (Region 14) (HM006 pSymA nt 602,640 – 623,487) Assembled by Yeast Recombineering into pTH3369 via PacI; Sp^R	**This Work**
pNDMS120	*pha-1* (Region 15) (HM006 pSymA nt 623,439 – 634,117) Assembled by Yeast Recombineering into pTH3369 via PacI; Sp^R	**This Work**
pNDMS121	*ctrl-2* (Region 16) (HM006 pSymA nt 633,590 – 641,765) Assembled by Yeast Recombineering into pTH3369 via PacI; Sp^R	**This Work**
pNDMS041	*att* (Region 08) (HM006 pSymA nt 641,749 – 660,572) *FRT*/FLP Excision Captured in M859 via Quadparental Mating Using RmND097 as Donor; Rf^R Km^R	**This Work**

pTH3369	BAC/YAC Multi-Host Shuttle Vector with *oriT*, *S. meliloti* pSymA with *FRT* and *attP* Sites; HIS3, Sp^R	**Geddes et al. 2021 (7)**
pNDMS250	pNDGG015 with HM006 pSymA nt 630,790 – 631,105 (GLND379/GLND380) via BsaI Golden Gate Cloning; Km^R	**This Work**
pNDMS303	pNDGG014 with HM006 pSymA nt 630,790 – 631,105 (GLND379/GLND380) via BsaI Golden Gate Cloning; Gm^R	**This Work**
pNDMS078	pNDGG015 with HM006 pSymA nt 628, 583 – 628,994 (GLND255/GLND256) via BsaI Golden Gate Cloning; Km^R	**This Work**
pNDMS073	pNDGG014 with HM006 pSymA nt 628, 583 – 628,994 (GLND255/GLND256) via BsaI Golden Gate Cloning; Gm^R	**This Work**
pNDMS252	pNDGG014 with HM006 pSymA nt 627,297 – 627,761 (GLND371/GLND372) via BsaI Golden Gate Cloning; Gm^R	**This Work**
pNDMS251	pNDGG015 with HM006 pSymA nt 625,031 – 625,675 (GLND375/GLND376) via BsaI Golden Gate Cloning; Km^R	**This Work**
pNDMS514	*ghbD* (HM006 pSymA nt 629,914 – 634,117) Assembled by Yeast Recombineering into pTH3369 via PacI; Sp^R	**This Work**
pNDMS515	*ghbD* & *attK* (HM006 pSymA nt 649,158 – 650,747 & HM006 pSymA nt 629,914 – 634,117) Assembled by Yeast Recombineering into pTH3369 via PacI; Sp^R	**This Work**

Supplemental Table S2. Summary of strains used in construction of individual deletions

Summary of Strains Used in Construction of Individual Deletions						
	First FRT Site Integration (Single Int.)			Second FRT Site Integration (Double Int.)		
Strain (Common Name)	**Background**	**Plasmid Integrated**	**Resulting Strain**	**Background**	**Plasmid Integrated**	**Resulting Strain**
RmND063 (Deletion 1)	RmP4566	pNDMS018	RmND053	RmND053	pNDMS020	RmND055
RmND064 (Deletion 2)	RmP4566	pNDMS019	RmND054	RmND054	pNDMS022	RmND056
RmND065 (Deletion 3)	RmP4566	pNDMS018	RmND053	RmND053	pNDMS021	RmND057
RmND101 (Deletion 4)	RmP4566	pNDMS021	RmND088	RmND088	pNDMS028	RmND093
RmND102 (Deletion 5)	RmP4566	pNDMS029	RmND089	RmND089	pNDMS028	RmND094
RmND103 (Deletion 6)	RmP4566	pNDMS029	RmND089	RmND089	pNDMS030	RmND095
RmND104 (Deletion 7)	RmP4566	pNDMS031	RmND090	RmND090	pNDMS030	RmND096
RmND105 (Deletion 8)	RmP4566	pNDMS031	RmND090	RmND090	pNDMS032	RmND097
RmND106 (Deletion 9)	RmP4566	pNDMS033	RmND091	RmND091	pNDMS032	RmND098
RmND107 (Deletion 10)	RmP4566	pNDMS033	RmND091	RmND091	pNDMS034	RmND099
RmND108 (Deletion 11)	RmP4566	pNDMS020	RmND092	RmND092	pNDMS034	RmND100
RmND199 (Deletion 14)	RmP4566	pNDMS090	RmND180	RmND180	pNDMS089	RmND183
RmND200 (Deletion 15)	RmP4566	pNDMS090	RmND180	RmND180	pNDMS091	RmND184
RmND201 (Deletion 16)	RmP4566	pNDMS031	RmND090	RmND090	pNDMS091	RmND185
RmND340 (Deletion 17)	RmP4566	pNDMS032	RmND292	RmND292	pNDMS160	RmND321
RmND365 (Deletion 18)	RmP4566	pNDMS160	RmND322	RmND322	pNDMS161	RmND342
RmND337 (Deletion 19)	RmP4566	pNDMS033	RmND091	RmND091	pNDMS161	RmND327

Supplemental Table S3. Primers for inserts used in plasmid construction

Primers for Inserts Used in Plasmid Construction					
Vector	**Primer**	**Forward**	**Primer**	**Reverse**	**Location**
pNDMS018 (KpnI/HindIII)	**BGND001**	AAAAAGCTTTTGAGAC CTCCAGCACTTCC	**BGND002**	AAAGGTACCAAACGAACAT GGACTTGGCC	HM006 pSymA nt 510,905 – 511,956
pNDMS019 (KpnI/HindIII)	**BGND005**	AAAAAGCTTCGTATGT GAGATTTTCGACGACA	**BGND006**	AAAGGTACCTGATGACAG GATTCCGTTGC	HM006 pSymA nt 1,173,460 – 1,174,283
pNDMS020 (BglII/PstI)	**BGND003**	AAACTGCAGTGTTCGT GCACCTCGGG	**BGND004**	AAAAGATCTTCATGTGGAT GCTTTGATGGC	HM006 pSymA nt 735,762 – 736,796
pNDMS021 (BglII/PstI)	**BGND007**	AAACTGCAGCTGGCGC TCGAGAAGGTG	**BGND008**	AAAAGATCTGATGGCCCG CAACGTCAT	HM006 pSymA nt 540,045 – 541,058
pNDMS022 (BglII/PstI)	**GLND009**	AAACTGCAGAAGTTGG CCGTTGACATCAG	**GLND010**	AAAAGATCTTCCATCTCGC ACTACAGAAGC	HM006 pSymA nt 1,366,931 – 1,368,079
pNDMS028 (KpnI/HindIII)	**GLND051**	AAAAAGCTTTTCTAACA TCGTTGGTCAGG	**GLND052**	AAAGGTACCCTGATCGCC AACCTCAAG	HM006 pSymA nt 549,073 – 549,894
pNDMS029 (BglII/PstI)	**GLND053**	AAACTGCAGGTGCTCT GGAATGTCTGC	**GLND054**	AAAAGATCTACTTCAGTGG CAGGTCA	HM006 pSymA nt 561,441 – 562,111
pNDMS030 (KpnI/HindIII)	**GLND055**	AAAAAGCTTCGGGACT TGTTATATGGGAG	**GLND056**	AAAGGTACCGTAGCTTTGA GGAGATGAGG	HM006 pSymA nt 580,735 – 581,373
pNDMS031 (BglII/PstI)	**GLND057**	AAACTGCAGGTTCATT GAAACGTGGATCA	**GLND058**	AAAAGATCTATTGCTGACG ACCCATCT	HM006 pSymA nt 641,749 – 642,320

pNDMS032 (KpnI/HindIII)	**GLND059**	AAAAAGCTTGATTGTTC CTCACCCTGTAG	**GLND060**	AAAGGTACCATAGAGCTTC CGCATGACA	HM006 pSymA nt 659,346 – 660,572
pNDMS033 (BglII/PstI)	**GLND061**	AAACTGCAGAAAGAGA GCGGCCCAAAAA	**GLND062**	AAAAGATCTGCATTCATTT GTCCCGAAC	HM006 pSymA nt 695,750 – 696,289
pNDMS034 (KpnI/HindIII)	**GLND063**	AAAAAGCTTAACAGGG TATGGCATCAAAG	**GLND064**	AAAGGTACCGCTGAACTG GTGGCTTCT	HM006 pSymA nt 719,140 – 719,868
pNDMS089 (KpnI/HindIII)	**GLND099**	AAAAAGCTTCGACAGT AGCATTTCACAAC	**GLND100**	AAAGGTACCGAGCATCCC TCGCAATAC	HM006 pSymA nt 602,640 – 603,904
pNDMS090 (BglII/PstI)	**GLND101**	AAACTGCAGCATCGTC CTCAACACTCTG	**GLND102**	AAAAGATCTGTCTCCTGAG TGTGTGTTT	HM006 pSymA nt 621,608 – 623,428
pNDMS091 (KpnI/HindIII)	**GLND103**	AAAAAGCTTAGTTCGA CGTCCGTCA	**GLND104**	AAAGGTACCCTTCCTTTCG TGCTTCAAAC	HM006 pSymA nt 634,974 – 635,363
pNDMS160 (BsaI GG)	**GLND265**	TTTGGTCTCTAAGCCTC TTCCTGATCGACCCA	**GLND266**	TTTGGTCTCTGGAGGATAA CGCACTCTCGACC	HM006 pSymA nt 679,739 – 680,027
pNDMS161 (BsaI GG)	**GLND267**	TTTGGTCTCTAAGCCA CCGAACATCAGCCATT	**GLND268**	TTTGGTCTCTGGAGTTCGA TTTTATCAGCCGCT	HM006 pSymA nt 685,776 – 686,199
gusA	**BGND059**	AAAGAAGACAATCCCG GTCTCAAATGGTCCGT CCT	**BGND060**	AAAGAAGACAATGCCGGT CTCAACCTTCATTGTTTGC CTCCC	pOPS0253 nt 734 – 2,546
pPha	**pPha F**	AAAGGTCTCAGGAGCA TACGGGCCGGCGG	**pPha R**	AAAGGTCTCACATTCGATG GAAATCCACCTTGCC	HM006 pSymA nt 632,983 – 633,911
pNDMS250 pNDMS303	**GLND379**	TTTGGTCTCAGGAGGG GTTTCTTGCGAGATAG G	**GLND380**	TTTGGTCTCTAGCGCGTCC AACATCCTTTTCGA	HM006 pSymA nt 630,790 – 631,105
pNDMS078 pNDMS073	**GLND255**	TTTGGTCTCAGGAGGC CAGCCATTTCTCCATG	**GLND256**	TTTGGTCTCTAGCGTCGAC GACTATATCCACGA	HM006 pSymA nt 628, 583 – 628,994
pNDMS252	**GLND371**	TTTGGTCTCAGGAGGC TGACGAAGGTGATAAT CT	**GLND372**	TTTGGTCTCTAGCGCTCTA CAAGACCTTCCCCAT	HM006 pSymA nt 627,297 – 627,761
pNDMS251	**GLND375**	TTTGGTCTCAGGAGCT GACCTTGTGCTTGTCG	**GLND376**	TTTGGTCTCTAGCGCCTCT ACCTGCCGATGAT	HM006 pSymA nt 625,031 – 625,675

Supplemental Table S4. Primers anchored in genome used for verification of plasmid integration into genome

Primers Anchored in Genome Used for Verification of Plasmid Integration into Genome				
Plasmid	**Primer**	**Forward**	**Primer**	**Reverse**
pNDMS018	**GLND013**	TTCATGTCATTCCCTCCTTG	**GLND016**	CGGAGTTGTCTGGGATTG
pNDMS019	**GLND017**	CATTGGTTTGAGAAGCGTAC	**GLND018**	GCGCCAAAACAGTCAAAA
pNDMS020	**GLND076**	ACGGGACTTCATAATGGAAC	**GLND024**	TTTTTCCTCTCCAACCACC
pNDMS021	**GLND068**	GGCCGATTAGTTTGCGAA	**GLND069**	TGTTTGTCGATCCGGGA
pNDMS022	**N/A**	N/A	**GLND025**	CTTCTGGAGTTCATCACGAA
pNDMS028	**GLND077**	GTTCTGAATCCATCCAAACG	**GLND078**	CAATCGCTATTTTCGTCTGC
pNDMS029	**GLND070**	CTAAACAGTCCGTCCATCAT	**GLND071**	GCGGACGATTACAACAATTT
pNDMS030	**GLND079**	AGGAACAAGAAGTGAACTCG	**GLND080**	GCAATGACTTACCTCCAAGA
pNDMS031	**GLND072**	GATTTGGGAGTGATGTTGGA	**GLND073**	GTCAAAGACCATTGCGAAG
pNDMS032	**GLND081**	CAGCCACTCGACATGATC	**GLND082**	TGGGATATGATGGCACTTTC
pNDMS033	**GLND137**	TAAAGTGTACCTAAACCCGC	**GLND138**	GTGACTTGGAGAAATTCGGT
pNDMS034	**GLND083**	GGAGCAGTATCGAGAAAAGT	**GLND084**	CCTGAGGAAATGTACGTAGG
pNDMS089	**GLND107**	GAGATCTGATTCATCCGAGT	**GLND108**	GCCGAGATGTGAACGAATA
pNDMS090	**GLND109**	TTCTAGGCTGAACTGCTGA	**GLND110**	CTCAAGTGGAATCTGACGAA
pNDMS091	**GLND111**	GAAGTGAACATGCCAGATTG	**GLND112**	ATTGACCTCCTTGACGTTC
pNDMS160	**GLND269**	GGTGCCAGGAAATCATAGAG	**GLND270**	TCTATCAGGAGAACCGCTT
pNDMS161	**GLND271**	CTCATCTTCGTCGCCTCA	**GLND272**	TTCGAATCTTGTTGGTGCAG
pNDMS250	**GLND381**	AAAGACGAGGGTGAGATTG	**GLND382**	GCTCTGCTCCGAATTTTAAC
pNDMS303	**GLND389**	CAGTTTCCCTTACCACATGA	**GLND390**	CTAGCCGACCGTAATAGTAG
pNDMS078	**GLND257**	ATAATCTTCTCTTCCGTCGC	**N/A**	N/A
pNDMS073	**GLND258**	CTCTTCCTGATCGACCCA	**N/A**	N/A
pNDMS252	**GLND373**	CTGAGATTGGATGCGATGT	**GLND374**	CAATCTCACCCTCGTCTTT
pNDMS251	**GLND377**	ATGCCATTCCCAAGCTTC	**GLND378**	CACTGGTTCAAGCCCTAC

Supplemental Table S5. Primers anchored in vectors used for verification of plasmid integration into genome

Primers Anchored in Vectors Used for Verification of Plasmid Integration into Genome				
Vector	**Primer**	**Forward**	**Primer**	**Reverse**
pTH1937	**GLND015**	ACTTGGTCTGACAGGAATTC	**GLND014**	GCGGAACCCCTATTTGTTTA
pTH3291	**GLND023**	TTCTGTTCATGGGGGTAATG	**GLND067**	GTCAAGGATCTGGATTTCGA
pNDGG014	**GLND218**	GCTGCTCCATAACATCAAAC	**GLND217**	TGTAGGTATCTCAGTTCGGT
pNDGG015	**GLND220**	CATCCAGTTTACTTTGCAGG	**GLND219**	GCGTAATCTCTTGCTCTGAA

Supplemental Table S6. Primer pairings for verification of plasmid integrations

Primer Pairings for Verification of Plasmid Integrations				
	Left Region Verification Pairing		**Right Region Verification Pairing**	
Plasmid	**Forward**	**Reverse**	**Forward**	**Reverse**
pNDMS018	GLND013	GLND014	GLND015	GLND016
pNDMS019	GLND017	GLND014	GLND015	GLND018
pNDMS020	GLND076	GLND067	GLND023	GLND024
pNDMS021	GLND068	GLND067	GLND023	GLND069
pNDMS022	N/A	N/A	GLND023	GLND025
pNDMS028	GLND077	GLND014	GLND015	GLND078
pNDMS029	GLND070	GLND067	GLND023	GLND071
pNDMS030	GLND079	GLND014	GLND015	GLND080
pNDMS031	GLND072	GLND067	GLND023	GLND073
pNDMS032	GLND081	GLND014	GLND015	GLND082
pNDMS033	GLND137	GLND067	GLND023	GLND138
pNDMS034	GLND083	GLND014	GLND015	GLND084
pNDMS089	GLND107	GLND014	GLND015	GLND108
pNDMS090	GLND109	GLND067	GLND023	GLND110
pNDMS091	GLND111	GLND014	GLND015	GLND112
pNDMS160	GLND269	GLND217	GLND218	GLND270
pNDMS161	GLND271	GLND219	GLND220	GLND272
pNDMS250	GLND381	GLND220	GLND219	GLND382
pNDMS303	GLND389	GLND218	GLND217	GLND390
pNDMS078	GLND257	GLND220	N/A	N/A
pNDMS073	GLND258	GLND218	N/A	N/A
pNDMS252	GLND373	GLND218	GLND217	GLND374
pNDMS251	GLND377	GLND220	GLND219	GLND378

Supplemental Table S7. Primer pairings for verification of the excision of flanked region (deletion verification)

Primer Pairings for Verification of the Excision of Flanked Region (Deletion Verification)			
Strain Name	**Common Name**	**Forward**	**Reverse**
RmND063	Deletion 1	GLND015	GLND024
RmND064	Deletion 2	GLND015	GLND025
RmND065	Deletion 3	GLND015	GLND026
RmND101	Deletion 4	GLND023	GLND078
RmND102	Deletion 5	GLND015	GLND071
RmND103	Deletion 6	GLND023	GLND080
RmND104	Deletion 7	GLND015	GLND073
RmND105	Deletion 8	GLND023	GLND082
RmND106	Deletion 9	GLND015	GLND075
RmND107	Deletion 10	GLND023	GLND085
RmND108	Deletion 11	GLND015	GLND024
RmND199	Deletion 14	GLND015	GLND110
RmND200	Deletion 15	GLND023	GLND112
RmND201	Deletion 16	GLND015	GLND073
RmND340	Deletion 17	GLND015	GLND270
RmND365	Deletion 18	GLND218	GLND272
RmND337	Deletion 19	GLND220	GLND138

Supplemental Table S8. Primers for inserts used in yeast recombineering

Primers for Inserts Used in Yeast Recombineering						
Plasmid		**Primer**	**Forward**	**Primer**	**Reverse**	**Location**
pNDMS119	**1**	**GLND157**	GCATAAAGCTTGCTCAATCAAT CACCGGATCCTTAATTAACGAC AGTAGCATTTCACAAC	**GLND158**	ATCCGAAGCCGTTGATGC	HM006 pSymA nt 602,640 – 607,411
	2	**GLND159**	CGTTGAAGTCAGGTGAGATA	**GLND160**	GCGTCCGAATTCTCAGTC	HM006 pSymA nt 607,369 – 611,744
	3	**GLND161**	CTCGTCCAATCATTACCGTT	**GLND162**	GAATCACGACCAGAGCCTAT	HM006 pSymA nt 611,705 – 615,737
	4	**GLND163**	CTAGCAGGCTGTTGAAAAAG	**GLND164**	CTTCAGTGTTCCCGTCAG	HM006 pSymA nt 615,687 – 618,790
	5	**GLND165**	CATCCGCCAACGTTCAATT	**GLND166**	CGCTATAATGACCCCGAAGCAGGG TTATGCAGCGGAAGATATCGAGAT AGGTGCCGTC	HM006 pSymA nt 618,752 – 623,487
pNDMS120	**1**	**GLND167**	GCATAAAGCTTGCTCAATCAAT CACCGGATCCTTAATTAACGAA CTCGCAAACTTCATC	**GLND168**	GATCAAGTGGTTCGAGGAG	HM006 pSymA nt 623,439 – 625,885
	2	**GLND169**	TCGACGCAATTATAGGAGAC	**GLND170**	TCACCAAAATCATAGCCGAA	HM006 pSymA nt 625,835 – 628,301
	3	**GLND171**	GTTATCCTATCCGTCTCGTG	**GLND172**	GTCATTCACATCGGATCTCA	HM006 pSymA nt 628,252 – 631,966
	4	**GLND173**	GAAATAGACCTGCTCCACTG	**GLND174**	CGCTATAATGACCCCGAAGCAGGG TTATGCAGCGGAAGATGAACAGAT AGGCAGGGTTTC	HM006 pSymA nt 631,919 – 634,117
pNDMS121	**1**	**GLND175**	GCATAAAGCTTGCTCAATCAAT CACCGGATCCTTAATTAACGGT CTTGTGTTTATTTCCG	**GLND176**	CCGACTTTAGGAGACCAAG	HM006 pSymA nt 633,590 – 638,011
	2	**GLND177**	CCAATCGTGCTGGTCAATAT	**GLND178**	CGCTATAATGACCCCGAAGCAGGG TTATGCAGCGGAAGATTCCACGTT TCAATGAACTGA	HM006 pSymA nt 637,939 – 641,765
pNDMS514	**1**	**GLND453**	GCATAAAGCTTGCTCAATCAAT CACCGGATCCTTAATTAAGAGA ATTCCGGTTGGTCGTC	**GLND174**	CGCTATAATGACCCCGAAGCAGGG TTATGCAGCGGAAGATGAACAGAT AGGCAGGGTTTC	HM006 pSymA nt 629,914 – 634,117
pNDMS515	**1**	**GLND455**	GCATAAAGCTTGCTCAATCAAT CACCGGATCCTTAATTAACTCAA TTCCTCCCTCATTGCC	**GLND456**	CGGCCATGACCCCGAGCTCGGAC GACCAACCGGAATTCTCGTCTTCT ACTGCGACGCGTC	HM006 pSymA nt 649,158 – 650,747
	2	**GLND457**	ATCAGAAGTGTCAAGTGCAAGA CGCGTCGCAGTAGAAGACGAG AATTCCGGTTGGTCGTC	**GLNF174**	CGCTATAATGACCCCGAAGCAGGG TTATGCAGCGGAAGATGAACAGAT AGGCAGGGTTTC	HM006 pSymA nt 629,914 – 634,117

Supplemental Table S9. Primers for verification of plasmids constructed by yeast recombineering

Primers for Verification of Plasmids Constructed by Yeast Recombineering					
Plasmid	**Spanning Fragments**	**Primer**	**Forward**	**Primer**	**Reverse**
pNDMS119	**3-4**	**GLND195**	CGCGATAATCCACCTTCAG	**GLND196**	GAACAGAAGGTCGTATTCCA
pNDMS120	**1-2**	**GLND197**	GACGTTCGCCCATTTCAT	**GLND198**	GCCGCATGTCTTCGAAAG
pNDMS121	**1-2**	**GLND199**	CTTCCTGTCCGACTACTATC	**GLND200**	CAGGTCATGCATATTCTCGA
pNDMS514	**V-1**	**GLND413**	GCACTTATCCCCAGGCTTGT	**GLND454**	CGTCGTTCATGTGATGCTGC
pNDMS515	**1-2**	**GLND458**	TTGGCTGAACTGGAATCGCT	**GLND459**	GTCCTGCCTTACGTGTTGGA

Supplemental Table S10. Top 50 Highly Expressed Genes on the HM006 pSymA (in HM006 pSymA hybrid) During Symbiosis with *M. sativa*. Genes highlighted in red represent *nif* genes, blue represents *fix* genes, and orange represents genes present in *pha-1* and *pha-2*.

Gene ID	TPM Counts	Annotation
gene-CDO22_RS20540	47457	*nifH*
gene-CDO22_RS20535	38162	*nifD*
gene-CDO22_RS20530	19574	*nifK*
gene-CDO22_RS20565	18971	*fixA*
gene-CDO22_RS36500	15403	*mosB*
gene-CDO22_RS21630	15070	
gene-CDO22_RS21635	14961	
gene-CDO22_RS20575	14385	*fixC*
gene-CDO22_RS20570	13162	*fixB*
gene-CDO22_RS20580	12098	*fixX*
gene-CDO22_RS20585	10352	*nifA*
gene-CDO22_RS20600	8430	*nifT*
gene-CDO22_RS20525	7202	*nifE*
gene-CDO22_RS22155	6556	
gene-CDO22_RS20590	6229	*nifB*
gene-CDO22_RS20520	6066	*nifX*
gene-CDO22_RS20790	6009	*fixK2*
gene-CDO22_RS20595	5740	*fdxN*
gene-CDO22_RS21640	3793	
gene-CDO22_RS21745	3281	
gene-CDO22_RS22040	3238	*mosF*
gene-CDO22_RS20510	3203	*fdxB*
gene-CDO22_RS19805	3145	*fixK*
gene-CDO22_RS20495	2992	*syrA*
gene-CDO22_RS22030	2899	*mosD*
gene-CDO22_RS22025	2893	*mosC*
gene-CDO22_RS20780	2559	*fixN2*
gene-CDO22_RS20370	2552	*nifN*
gene-CDO22_RS22145	2545	
gene-CDO22_RS22035	2247	*mosE*
gene-CDO22_RS22150	2187	
gene-CDO22_RS20775	2170	*fixO2*
gene-CDO22_RS21750	2056	
gene-CDO22_RS21600	1840	
gene-CDO22_RS21915	1835	
gene-CDO22_RS19810	1782	*fixM*
gene-CDO22_RS21580	1755	*acs*
gene-CDO22_RS21650	1689	
gene-CDO22_RS36445	1480	
gene-CDO22_RS21300	1430	*groES*
gene-CDO22_RS22140	1364	
gene-CDO22_RS23035	1358	
gene-CDO22_RS21645	1318	
gene-CDO22_RS21590	1131	*phaC*
gene-CDO22_RS20765	1062	*fixP2*
gene-CDO22_RS21260	1047	
gene-CDO22_RS21585	1028	
gene-CDO22_RS23475	1010	
gene-CDO22_RS25040	934	
gene-CDO22_RS21755	885	

Supplemental Table S11. Top 50 BlastN hits using HM006 *phaC2* (CDO22_RS2690) as query (April 2024)

Description	Query Cover	E value	Per. ident	Accession
Sinorhizobium meliloti strain HM006 plasmid psymA, complete sequence	100%	0	100	CP021830.1
Sinorhizobium meliloti strain RCAM1115 plasmid p_1, complete sequence	100%	0	99.28	CP050559.1
Sinorhizobium meliloti strain RCAM1115 plasmid p_3, complete sequence	100%	0	98.74	CP050560.1
Sinorhizobium meliloti strain USDA1963 plasmid pHRB800, complete sequence	100%	0	97.56	CP011000.1
Sinorhizobium meliloti strain L6-AK89 plasmid pL6-AK89, complete sequence	100%	0	94.5	CP085526.1
Sinorhizobium meliloti strain ml45 plasmid pMl2, complete sequence	100%	0	94.4	CP140962.1
Sinorhizobium meliloti strain ml45 chromosome, complete genome	100%	0	94.4	CP140960.1
Sinorhizobium meliloti strain ml59 chromosome, complete genome	100%	0	94.4	CP140949.1
Sinorhizobium meliloti strain ml21 plasmid pMl1, complete sequence	100%	0	94.4	CP140939.1
Sinorhizobium meliloti strain ml21 chromosome, complete genome	100%	0	94.4	CP140938.1
Rhizobium leguminosarum bv. viciae strain BIHB 1217 plasmid pPR4, complete sequence	99%	0	90.24	CP022669.1
Rhizobium sp. NZLR1 plasmid p3, complete sequence	99%	0	90.24	CP071635.1
Rhizobium leguminosarum bv. viciae plasmid pRL10 complete genome, strain 3841	100%	0	89.88	AM236084.1
Rhizobium sullae strain WSM1592 plasmid pWSM1592_2, complete sequence	100%	0	88.92	CP104145.1
Rhizobium leguminosarum strain GLR17 chromosome, complete genome	100%	0	88.74	CP071626.1
Rhizobium indicum strain JKLM 13E plasmid pPR13E04, complete sequence	100%	0	88.62	CP054035.1
Rhizobium indicum strain JKLM 12A2 plasmid pPR12A203, complete sequence	100%	0	88.62	CP054024.1
Rhizobium hidalgonense strain JKLM 19E plasmid pPR19E03	100%	0	88.44	CP054030.1
Rhizobium leguminosarum strain CC283b plasmid pCC283b_4, complete sequence	95%	0	89.1	CP121639.1
Rhizobium leguminosarum strain Ta6k plasmid pRL7, complete sequence	95%	0	89.1	CP090199.1
Rhizobium leguminosarum strain Ta9k plasmid pRL3, complete sequence	95%	0	89.1	CP090115.1
Rhizobium leguminosarum strain Ta1k plasmid pRL3, complete sequence	95%	0	89.1	CP090108.1
Rhizobium leguminosarum strain Vaf10 plasmid unnamed1, complete sequence	100%	0	87.57	CP016287.1
Rhizobium lentis strain BLR27 plasmid p4, complete sequence	100%	0	87.48	CP071458.1
Rhizobium leguminosarum strain Tp73_4 plasmid pRLTp73_2, complete sequence	99%	0	87.16	CP090100.1
Rhizobium johnstonii strain TP5 plasmid pRlX2, complete sequence	99%	0	87.41	CP140821.1
Rhizobium johnstonii strain TP60 plasmid pRlX3, complete sequence	99%	0	87.33	CP140804.1
Rhizobium johnstonii strain TP25 plasmid pRlX4, complete sequence	99%	0	87.1	CP140849.1
Rhizobium beringeri strain TP6 plasmid pRlX2, complete sequence	99%	0	87.1	CP140809.1
Rhizobium beringeri strain TP66 plasmid pRlX4, complete sequence	99%	0	87.1	CP140800.1
Rhizobium ruizarguesonis strain TP15 plasmid pRlX1, complete sequence	97%	0	87.17	CP140869.1
Rhizobium ruizarguesonis strain TP33 plasmid pRlX1, complete sequence	97%	0	87.17	CP140841.1
Rhizobium ruizarguesonis strain TP42 plasmid pRlX3, complete sequence	97%	0	87.17	CP140833.1
Rhizobium ruizarguesonis strain TA1 plasmid pTA1_4, complete sequence	97%	0	87.17	CP088108.1
Rhizobium leguminosarum strain ATCC 14479 plasmid unnamed2, complete sequence	99%	0	87	CP030762.1
Rhizobium ruizarguesonis strain TP23 plasmid pRlX3, complete sequence	99%	0	87.13	CP140859.1
Rhizobium beringeri strain TP24 plasmid pRlX3, complete sequence	99%	0	87.13	CP140854.1
Rhizobium ruizarguesonis strain TP53 plasmid pRlX1, complete sequence	97%	0	87.17	CP140815.1
Rhizobium beringeri strain TP37 plasmid pRlX1, complete sequence	99%	0	87.13	CP140836.1
Mesorhizobium sp. M3A.F.Ca.ET.080.04.2.1 chromosome, complete genome	96%	0	82.4	CP034451.1
Bosea vaviloviae strain Vaf18 plasmid unnamed1, complete sequence	96%	0	81.84	CP017148.1
Bosea sp. F3-2 chromosome, complete genome	96%	0	81.44	CP042331.1
Bradyrhizobium sp. 2S1 strain 26S5 chromosome, complete genome	94%	0	76.67	CP145948.1
Bradyrhizobium sp. CB82 chromosome, complete genome	92%	0	76.5	CP121650.1

Bradyrhizobium arachidis strain SM32 chromosome, complete genome	89%	0	76.81	CP077970.1
Bradyrhizobium diazoefficiens strain XF7 chromosome, complete genome	86%	0	77.15	CP029603.2
Bradyrhizobium prioritasuperba strain BL16A chromosome, complete genome	86%	0	76.61	CP135921.1
Bradyrhizobium canariense strain WU425 chromosome, complete genome	87%	0	76.4	CP088089.1
Bradyrhizobium sp. 40 chromosome, complete genome	88%	0	75.97	CP064688.1
Bradyrhizobium sp. BWC-3-1 chromosome, complete genome	87%	0	75.78	CP136625.1

Supplemental Table S12. Genome resequencing data from *S. meliloti* pSymA and pSymB hybrid strains

Sample Name	Filter Reads Count	Mean Depth, X	Chromosome coverage NC_003047	Plasmid 1 (pSymA)	Plasmid 1 coverage	Plasmid 2 (pSymB)	Plasmid 2 coverage	SNPs	Indels
Rm5000	7135526	145.61	100.00%	NC_003037	99.91%	NC_003078	100.00%	66	78
RmP110	9272094	187.62	100.00%	NC_003037	99.93%	NC_003078	100.00%	64	77
RmP4393	9145658	189.56	97.87%	NC_009621	100.00%	NC_003078	100.00%	34	56
RmP4410	13501428	272.72	97.88%	NC_003037	99.94%	NC_003078	100.00%	65	81
RmP4411	11317880	229.89	97.88%	CP021798	100.00%	NC_003078	100.00%	32	59
RmP4412	9247792	183.55	97.87%	CP021830	100.00%	NC_003078	100.00%	35	58
RmP4414	8854212	175.39	97.90%	CP021805	100.00%	NC_003078	100.00%	122	59
RmP4417	3788872	76.51	97.86%	CP021824	99.99%	NC_003078	99.99%	35	57
RmP4452	9961874	208.31	97.87%	NC_009621	100.00%	NC_009620	100.00%	25	13
RmP4453	4298730	89.66	97.88%	NC_003037	99.84%	NC_009620	100.00%	56	36
RmP4459	9656590	196.77	97.88%	NC_003037	99.93%	CP021831	100.00%	85	36
RmP4460	3927642	79.14	97.83%	CP021830	100.00%	CP021831	99.98%	51	14

Supplemental Table S13. Accessions for raw data deposited to NCBI short read archive

Sequencing Project Name	NCBI Bioproject	NCBI Biosample	SRA Project Accession	SRA Run Accession
Sinorhizobium meliloti Rm5000 resequencing	PRJNA1109920	SAMN41306797	SRP509585	SRR29155454
Sinorhizobium meliloti RmP110 resequencing	PRJNA1109919	SAMN41306793	SRP509575	SRR29155423
Sinorhizobium meliloti RmP4393 resequencing	PRJNA1109917	SAMN41306788	SRP509579	SRR29155438
Sinorhizobium meliloti RmP4410 resequencing	PRJNA1109902	SAMN41306366	SRP509658	SRR29155557
Sinorhizobium meliloti RmP4411 resequencing	PRJNA1109905	SAMN41307501	SRP509659	SRR29155556
Sinorhizobium meliloti RmP4412 resequencing	PRJNA1109911	SAMN41306778	SRP509580	SRR29155441
Sinorhizobium meliloti RmP4414 resequencing	PRJNA1109914	SAMN41306364	SRP509573	SRR29155412
Sinorhizobium meliloti RmP4417 resequencing	PRJNA1109908	SAMN41306785	SRP509582	SRR29155447
Sinorhizobium meliloti RmP4452 resequencing	PRJNA1109918	SAMN41306373	SRP509572	SRR29155394
Sinorhizobium meliloti RmP4453 resequencing	PRJNA1109916	SAMN41306374	SRP509577	SRR29155428
Sinorhizobium meliloti RmP4459 resequencing	PRJNA1109910	SAMN41306784	SRP509584	SRR29155449
Sinorhizobium meliloti RmP4460 resequencing	PRJNA1109912	SAMN41306780	SRP509576	SRR29155425
Medicago sativa/Sinorhizobium meliloti RmP4566 co-culture transcriptomics	PRJNA1109882	SAMN41306367	SRP509638	SRR29155541

Medicago sativa/Sinorhizobium meliloti RmP4566 co-culture transcriptomics	PRJNA1109883	SAMN41306365	SRP509639	SRR29155539
Medicago sativa/Sinorhizobium meliloti RmP4566 co-culture transcriptomics	PRJNA1109884	SAMN41306796	SRP509640	SRR29155540
Medicago sativa/Sinorhizobium meliloti RmP4566 co-culture transcriptomics	PRJNA1109882	SAMN41306367	SRP509638	SRR29155541

Supplemental Figures

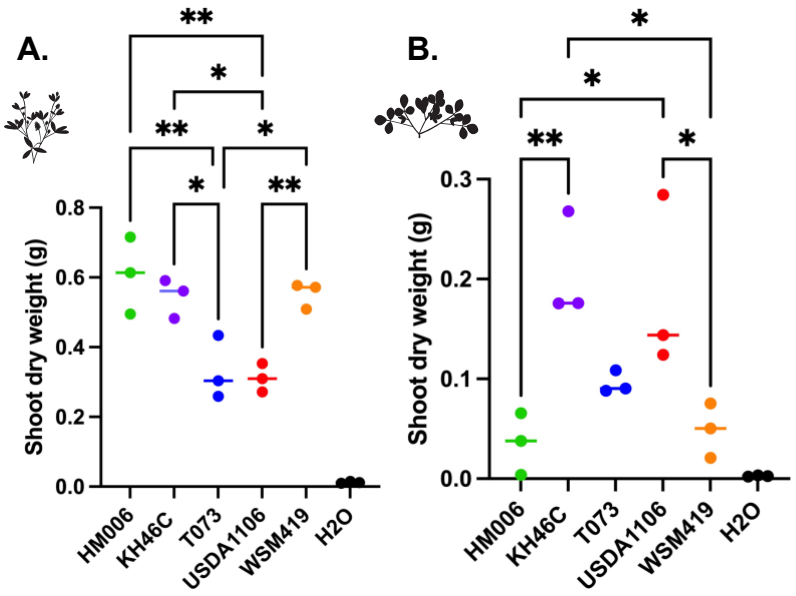

Supplemental Figure S1. Variations in partner quality phenotypes of Sinorhizobium strains based on shoot dry weight accumulation in nitrogen-limiting conditions. Shoot dry weight accumulation in *M. sativa* cv. *Iroquois* (**A**) and *M. truncatula* A17 (**B**) inoculated with different strains of *S. meliloti* and *S. medicae*.

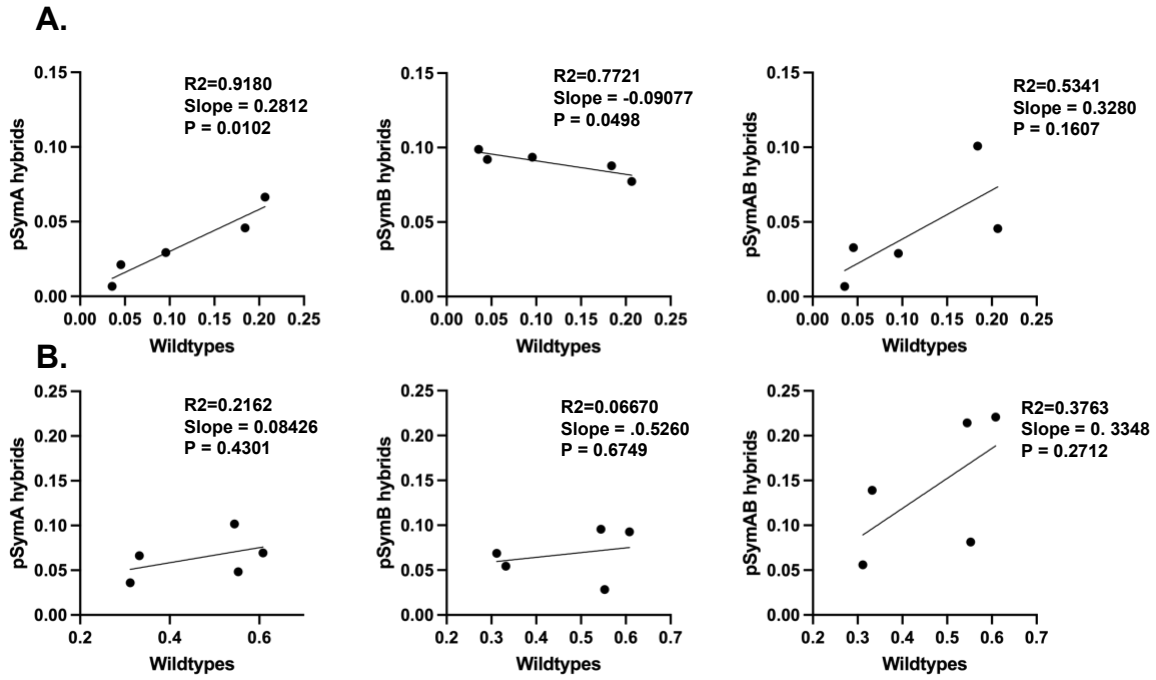

Supplemental Figure S2. Correlations between shoot biomass production of natural strains and hybrid strains derived from transform of pSymA, pSymB or both pSymA and pSymB replicons to a common background. The data are derived from *Sinorhizobium meliloti* HM006, T073, USDA1106, KH46 and *Sinorhizobium medicae* WSM419 wildtype strains, with hybrids containing the stated replicons from each strain in an Rm5000 background. Data was collected as shoot dry weight production during isogenic inoculation of *Medicago sativa* cv. Iroquois (**A**), and *Medicago truncatula* A17 (**B**)

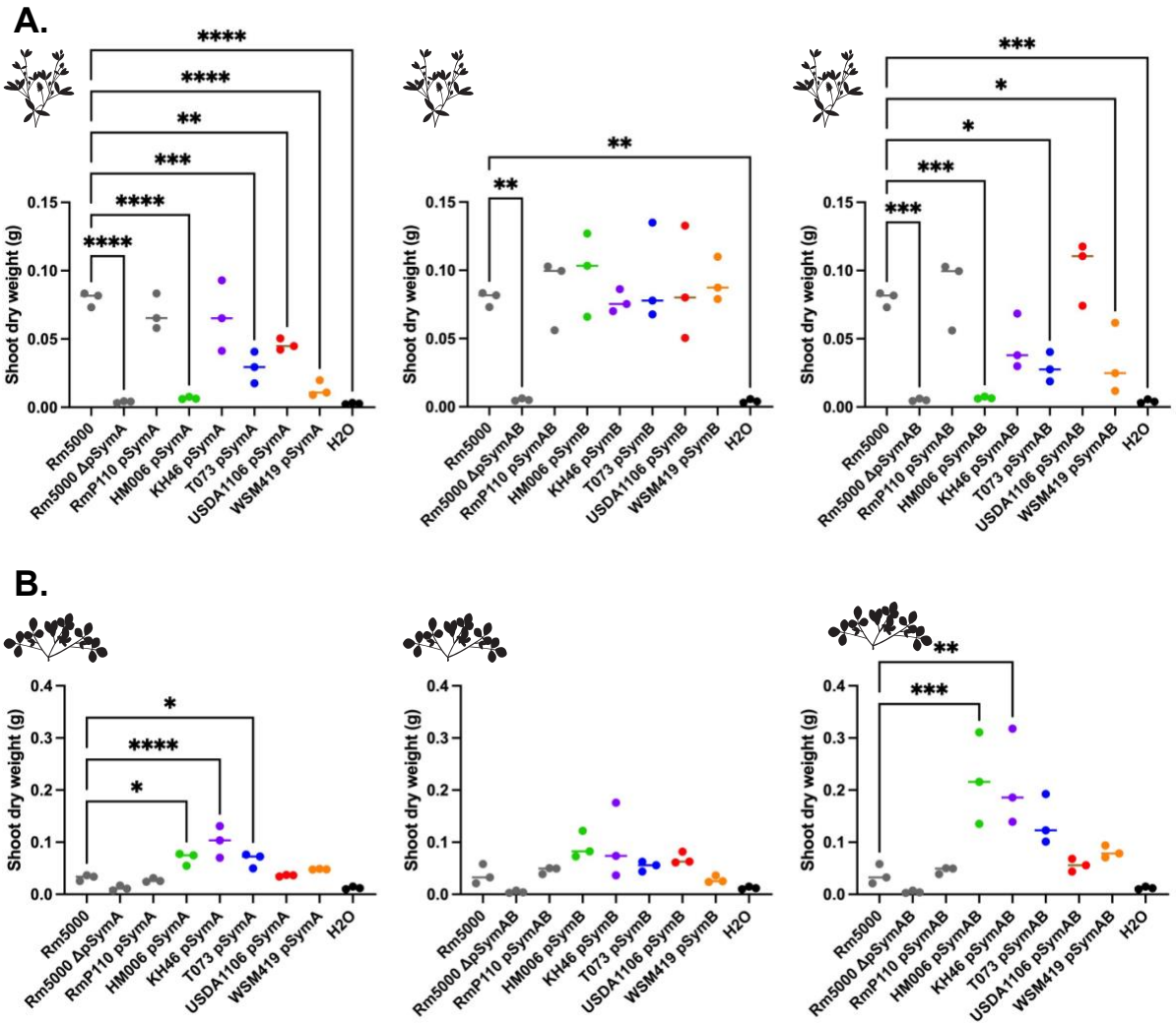

Supplemental Figure S3. Changes in the partner quality phenotypes of Rm5000 by the introduction of heterologous pSymA, pSymB or pSymA and pSymB replicons. Shoot dry weight accumulation in *M. sativa* cv. *Iroquois* (**A**) and *M. truncatula* A17 (**B**) inoculated with different strains of *S. meliloti* Rm5000 bearing heterologous pSymAs, pSymBs, or both from *Sinorhizobium meliloti* RmP110 (near isogenic), HM006, T073, USDA1106, KH46 and *Sinorhizobium medicae* WSM419 wildtype strains.

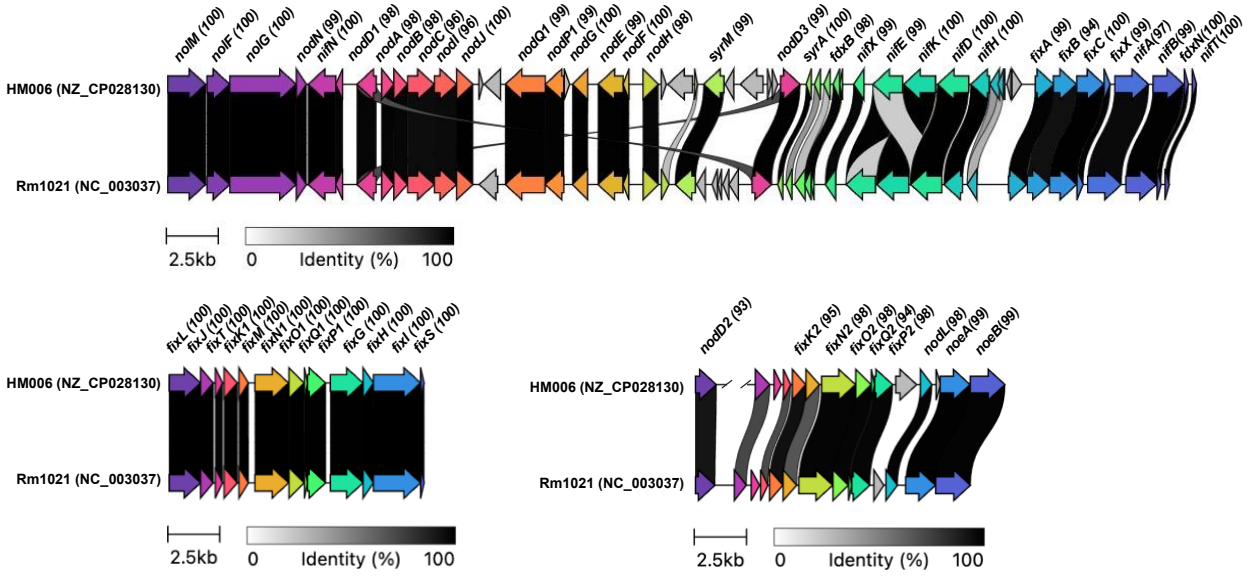

Supplemental Figure S4. Homology between *nod*, *nif*, and *fix* loci from HM006 and Rm1021. Alignment of HM006 and Rm1021 *nod*, *nif* and *fix* clusters using clinker (Min. alignment sequence identity 0.3), visualized with clustermap.js (>0.5 alignment sequence identity shown). Intensity of connecting lines indicates percent identity between genes (more intense lines indicated higher identity).

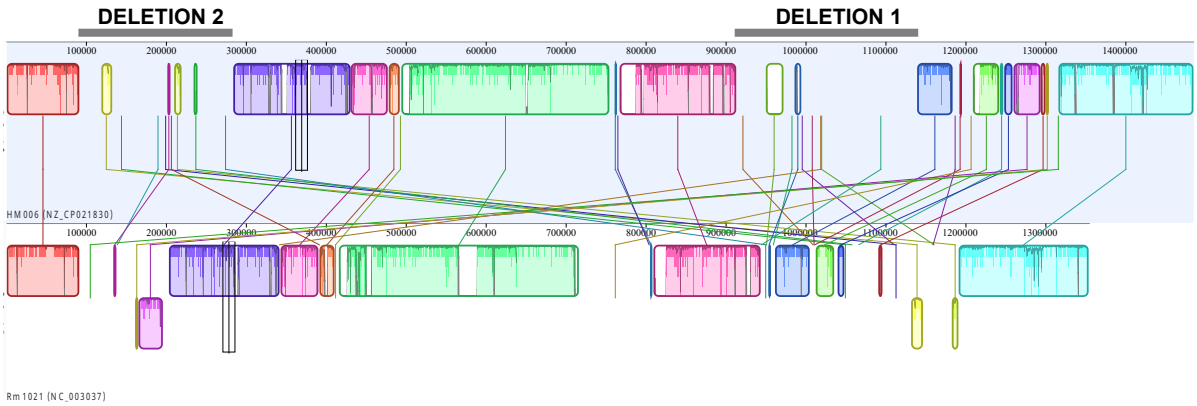

Supplemental Figure S5. MAUVE alignments between HM006 and *S. meliloti* strains in this study. Alignment of pSymAs from *S. meliloti* HM006 and Rm1021 with locally colinear gene blocks between them as colored boxes.

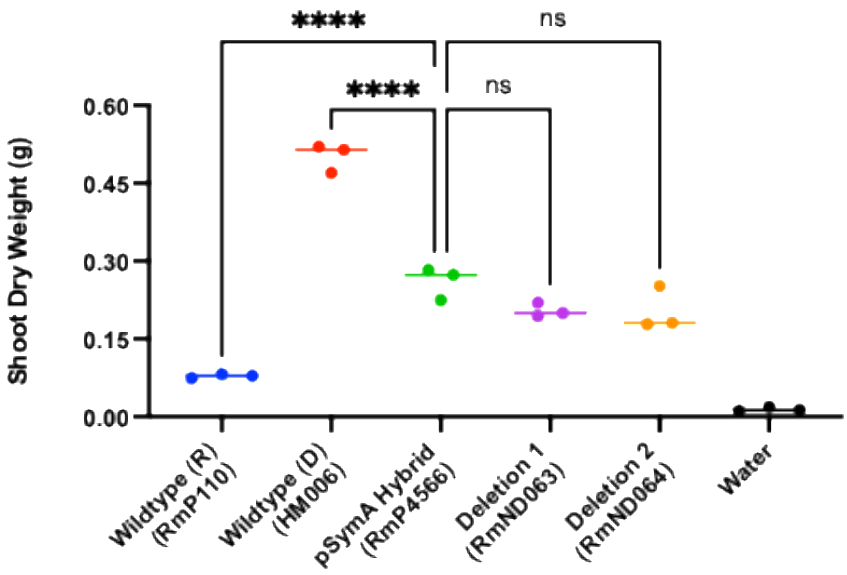

Supplemental Figure S6. Neither Deletion 1 nor Deletion 2 affected symbiosis with *M. truncatula* compared to the HM006 pSymA-Hybrid. Quantitation of shoot dry weight accumulation by *M. truncatula* inoculated with wildtype RmP110, HM006, HM006 pSymA-Hybrid, Deletion 1, Deletion 2, and water control.

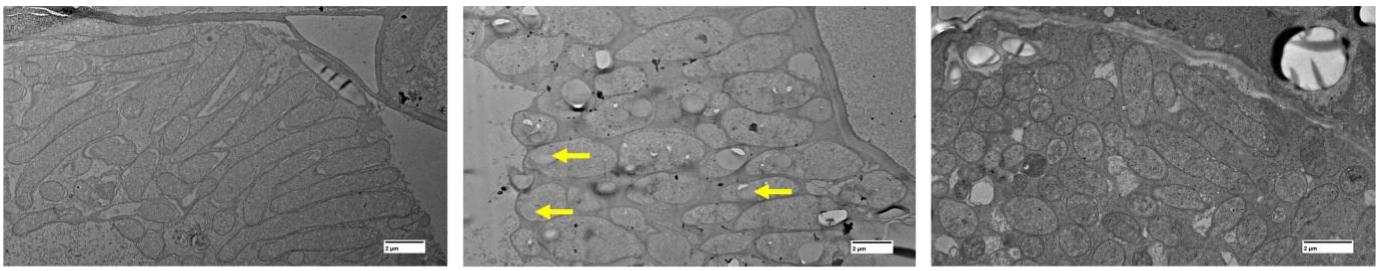

Supplemental Figure S7. Evidence for PHA granules in *Medicago truncatula* nodules.
Nodules of *M. truncatula* A17 inoculated with wildtype (left), HM006 pSymA-Hybrid (middle), and Deletion 1 (right) were fixed 42 days post inoculation and used for electron microscopy. PHA granules display as light gray circles. Yellow arrows point to examples of PHA granules in bacteroids. Wildtype and Deletion 1 are devoid of PHA granules while the HM006 pSymA-Hybrid displays large PHA granules.

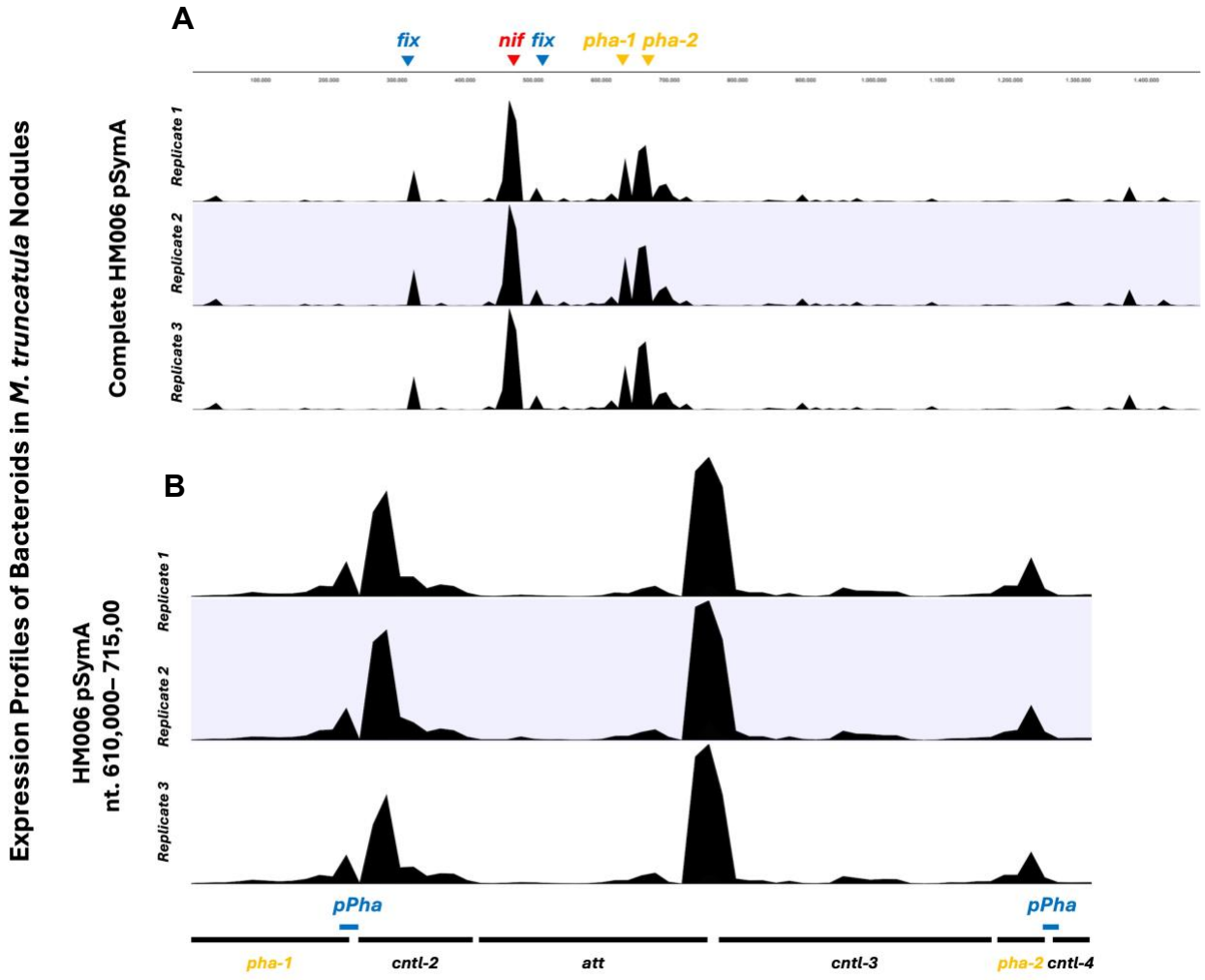

Supplemental Figure S8. Transcriptome profile (RNAseq count) across the complete HM006 pSymA replicon in bacteroids from *M. truncatula* nodules. Transcription profile (RNAseq count) across the complete pSymA HM006 replicon (in HM006-pSymA hybrid) in bacteroids from nodules of *M. truncatula*. *fix* and *nif* genes are marked to show relative expression levels with respect to genes in *pha-1* and *pha-2*. Orange highlighted genes represent the putative operons found in *pha-1* and *pha-2*. (**A**) Showing expression levels across complete pSymA. (**B**) Showing expression levels across zoomed in region of HM006 pSymA from nt. 610,000 – 715,000.

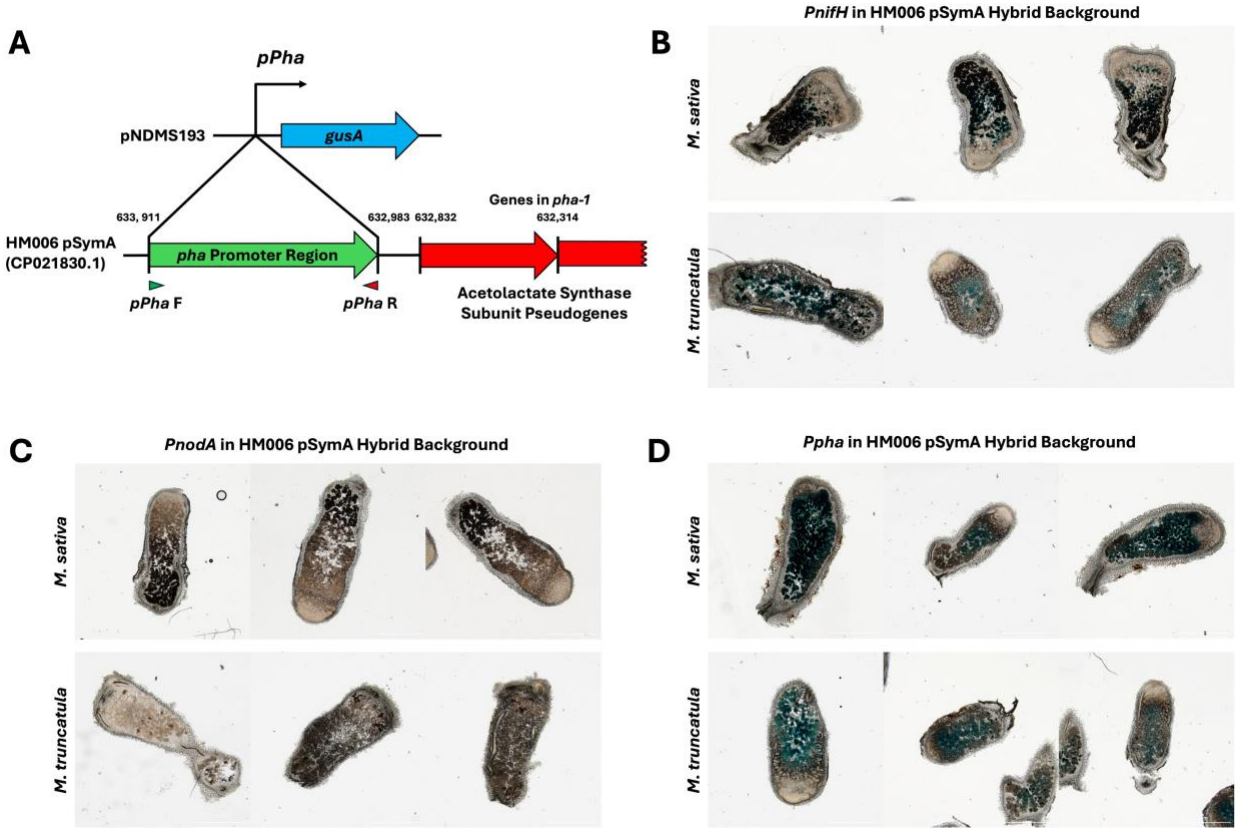

Supplemental Figure S9. Diagram of *Ppha* region fused with gusA and corresponding expression in various *S. meliloti* backgrounds in *M. sativa* and *M. truncatula* nodules. (A) Diagram displaying specific region deemed "*Ppha*" within *pha-1* operon driving gusA expression. *M. truncatula* and *M. sativa* nodule cross-sections harvested 42 days post inoculation displaying gusA expression driven by *nifH* (positive control) (**B**), *nodA* (negative control) (**C**), and *Ppha* (**D**) promoter region in HM006 pSymA hybrid.

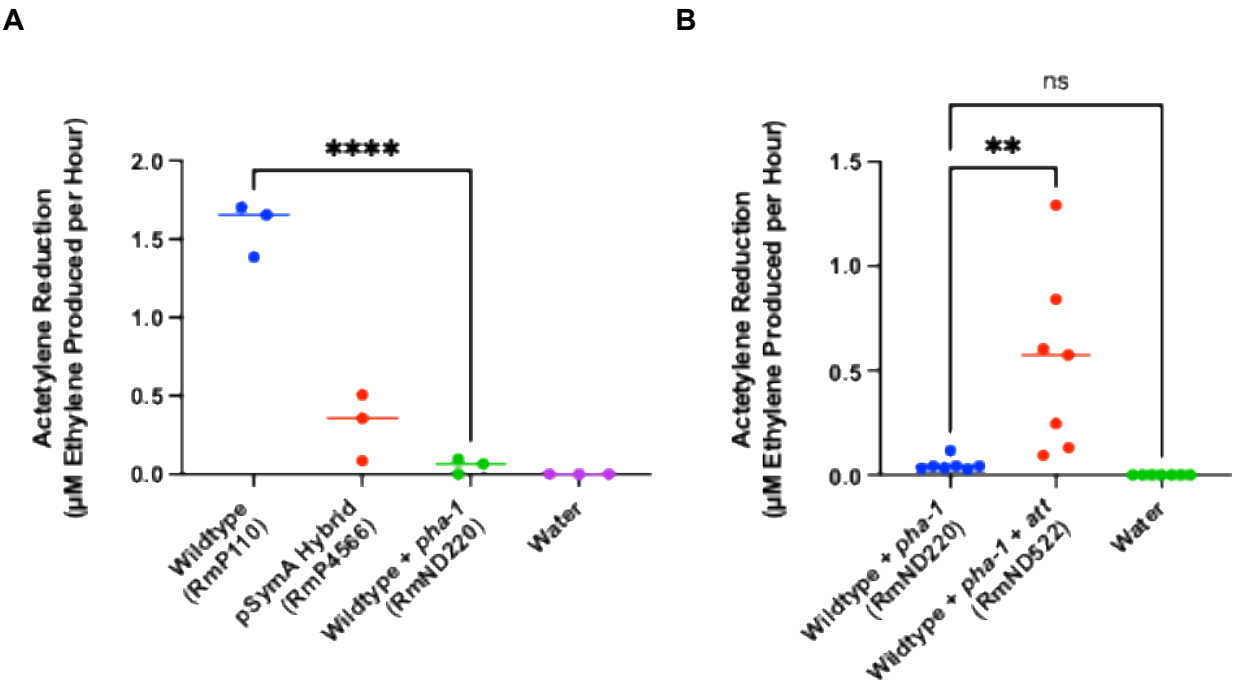

Supplemental Figure S10. Acetylene reduction activity of RmP110 with *pha-1* alone and *pha-1* with catabolism genes. Wildtype + *pha-1* fixed acetylene at nearly undetectable levels as fixation rates were comparable to the water control which had undetectable ethylene peaks. The inclusion of *att* rescued the strain to fix nitrogen. **(A)** Acetylene reduction activity of alfalfa inoculated with wildtype RmP110, HM006 pSymA Hybrid, wildtype + *pha-1*, and water control. **(B)** Acetylene reduction activity of alfalfa inoculated with wildtype + *pha-1*, wildtype + *pha-1* + *att*, and water control. **(A and B)** Each dot represents one replicate comprised of six alfalfa plants. Data is displayed as µM of ethylene produced per hour per jar containing one replicate. Ethylene peaks were undetectable for water controls, leading to the graphical representation of 0 µM ethylene produced per hour.

Supplemental Figure S11. Signs of degradation within alfalfa nodule occupied by wildtype + *pha-1*. TEM image of *M. sativa* nodule cross-section harvested 42 days post inoculation with wildtype + *pha-1*. Red arrows point to large PHA granules displaying as light gray circles. Blue arrows point to bacteroids with signs of degradation including dark coloration or being devoid of internal contents.

A

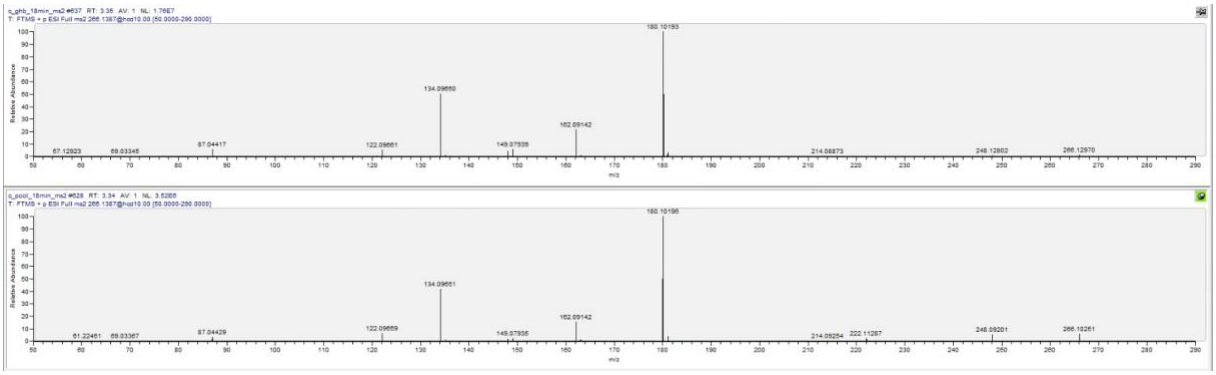

B

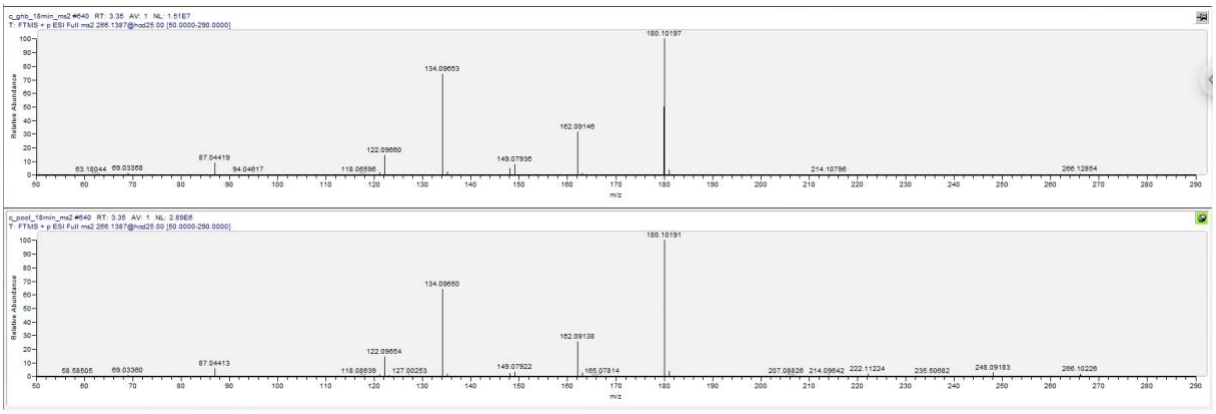

C

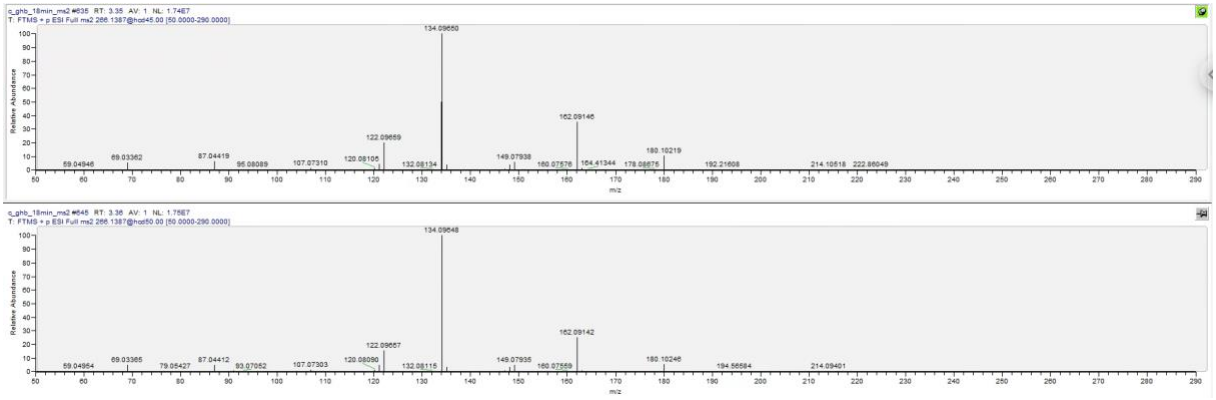

Supplemental Figure S12. Verification of Gamma-Hydroxybutyrate Identification from *Medicago sativa* nodules containing HM006 pSymA hybrid bacteroids. Verification of the key compound gamma-hydroxybutyrate (GHB) was performed using an authentic standard on an alternative instrumental platform. Specifically, MS/MS spectra and retention time (RT) data from the samples were compared to those of the standard, both acquired on a Dionex 3000 LC system coupled with Orbitrap Q Exactive HF mass spectrometer (ThermoFisher, Waltham, MA,

US), using the same LC method and column. The MS/MS spectra of GHB in the samples, collected at multiple collision energies, matched those of the authentic standard, confirming the compound's identity in the sample. **(A)** MS/MS spetra comparison between the GHB standard (top) and sample targets (bottom) using Higher-energy Collisional Dissociation (HCD) at 10 eV. **(B)** MS/MS spetra comparison between the GHB standard (top) and sample targets (bottom) using Higher-energy Collisional Dissociation (HCD) at 25 eV. **(C)** MS/MS spetra comparison between the GHB standard (top) and sample targets (bottom) using Higher-energy Collisional Dissociation (HCD) at 50 eV.

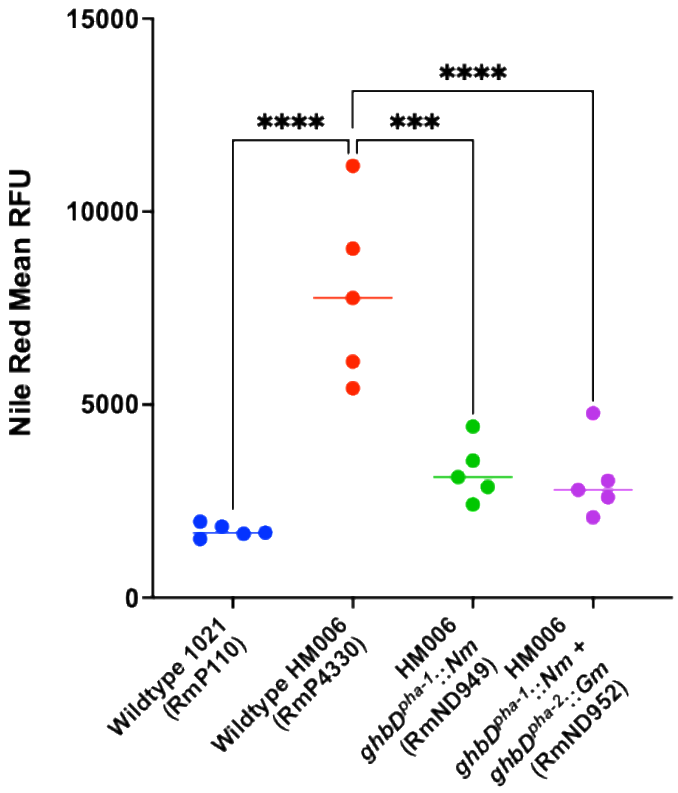

Supplemental Figure S13. Quantification of PHA production by Nile Red straining of bacteroids collected from *M. truncatula* nodules occupied by HM006 and HM006 *ghbD* mutants. Mean Nile Red values of isolated bacteroids from 42-day old *M. truncatula* nodules**.** Inoculants included wildtype, HM006 wildtype, HM006 *ghbD*$^{pha-1}$::*Nm* mutant and HM006 *ghbD*$^{pha-1}$::*Nm* + *ghbD*$^{pha-2}$::*Gm* mutant.

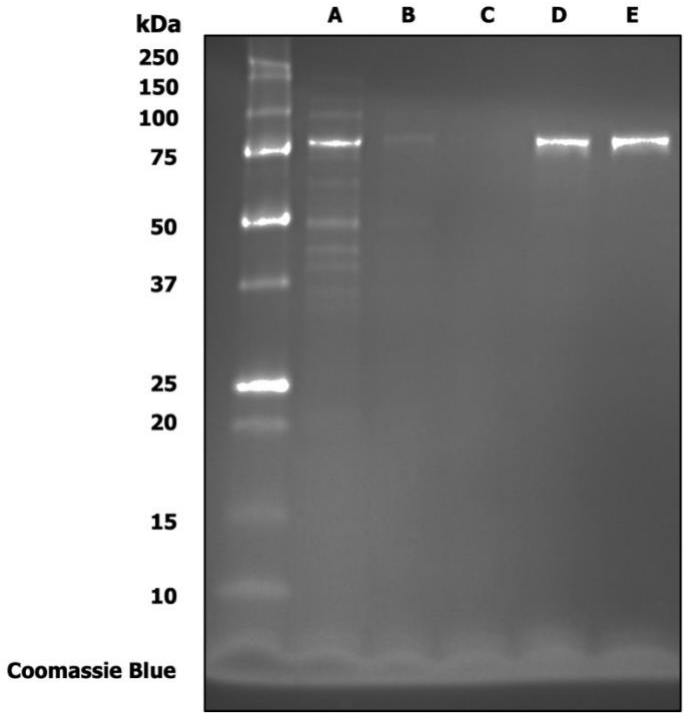

Supplemental Figure S14. Polyacrylamide gel electrophoresis of various fractions of GhbD purification process. The following are specific fractions of the ghbD purification process represented in lanes A-E: (A) 1:10 dilution of filtered cell-lysis, (B) 1:10 dilution of unbound, (C) wash, (D) pure ghbD prior to buffer exchange, and (E) pure ghbD after buffer exchange. ghbD is estimated as 42 kDa and the 6xHIS MBP tag is estimated as 44 kDa. The complete protein, ghbD with a 6xHIS MBP tag, is estimated as 86 kDa.

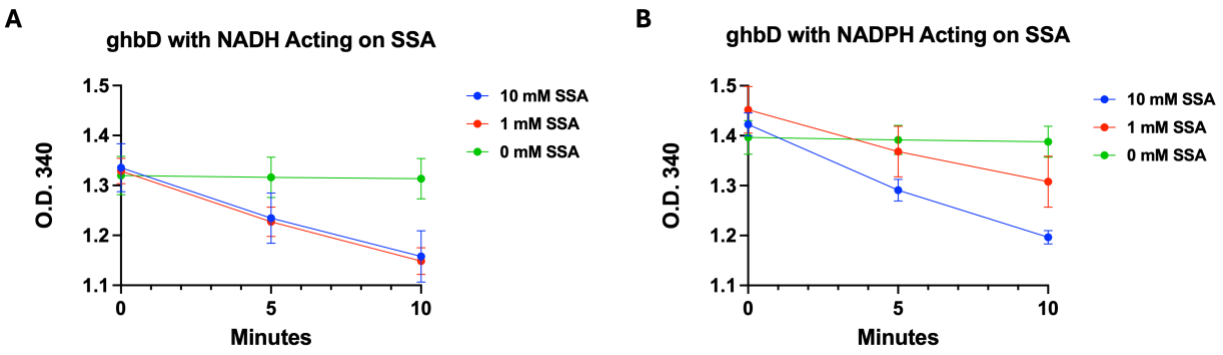

Supplemental Figure S15. Change in optical density over time of reactions between GhbD and varying concentrations of SSA with either NADH or NADPH. No change in optical density in reactions containing 0 mM SSA indicates no background activity in reaction mixture leading to conversion of either NADH or NADPH to NAD or NADP, respectively. Graphs represent change in optical density caused by use of either NADH **(A)** or NADPH **(B)** in reaction between GhbD and concentrations of 0 mM, 1 mM, and 10 mM SSA.

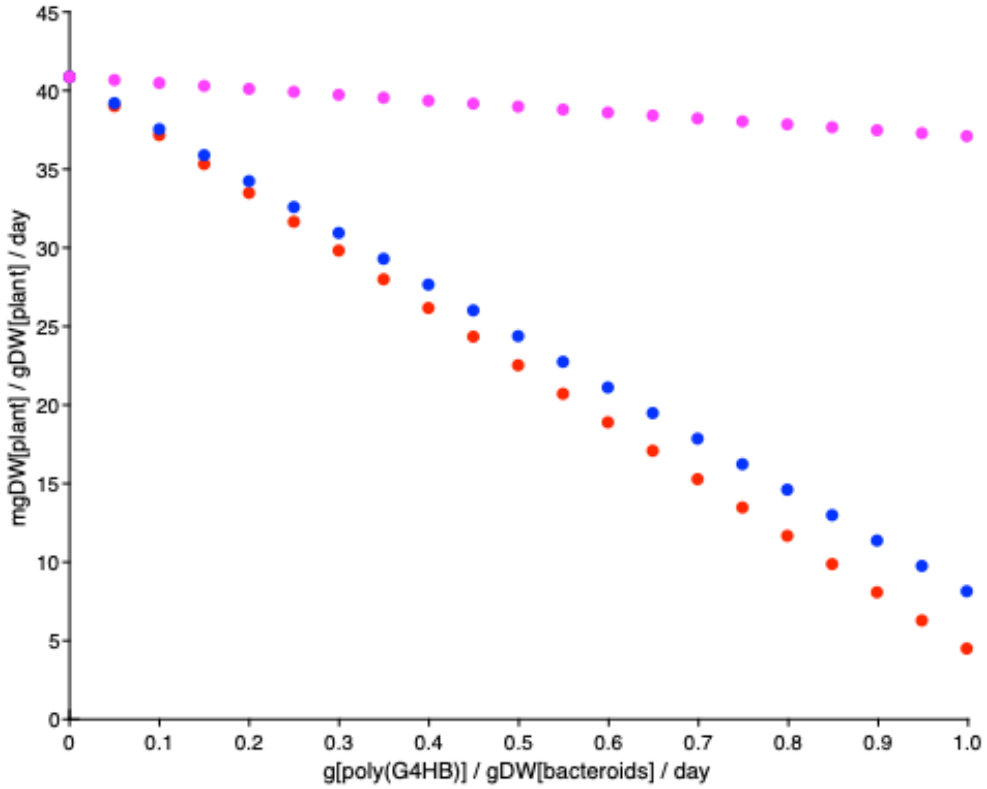

Supplemental Figure S16. Simulated metabolic effects of *ghbD* overexpression on a *Sinorhizobium – Medicago* symbiosis. The metabolic consequences of over-expressing *ghbD* on the symbiosis was investigated using ViNE (32), a genome-scale metabolic model for simulating the metabolism of a *S. meliloti* nodulated *M. truncatula* plant. As the metabolite succinate semialdehyde is not present in the bacteroid component of ViNE, the effects of GhbD in zone III nitrogen-fixing bacteriods were instead simulated through increasing the flux through an added sink reaction that removes either: consumed succinic acid, NADH, and H+, and produced NAD+ (red); consumed succinic acid (blue); or consumed NADH and H+ and produced NAD+ (magenta). Plant growth rate, expressed as the rate of total plant dry mass (mg) produced per gram of plant dry mass per day is shown on the Y-axis, while the X-axis shows the rate of poly(G4HB) production per gram of bacteroid dry mass per day. The results are consistent with increasing poly(G4HB) production decreasing the rate of nitrogen fixation and thus plant shoot dry weight accumulation, primarily through the diversion of carbon from the TCA cycle rather than the oxidation of available reductant. However, the results also suggest that the complete loss of nitrogen-fixation by *S. meliloti* bacteriods synthesizing poly(G4HB) in *M. sativa* nodules is unlikely to be explained by the diversion of carbon from the TCA cycle, as the amount of poly(G4HB) that would need to be continuously synthesized to produce this result

is physiologically unrealistic; even if bacteriods produced their own weight in poly(G4HB) every two days (which would require the diversion of 31% of imported succinate away from the TCA cycle), the rate of plant growth is predicted to decrease by only 45%. Consequently, the collapse of *M. sativa* symbiosis that was experimentally observed is unlikely to be due to the diversion of carbon from central metabolism, and may instead be due to other reasons, such as toxicity due to the buildup of poly(G4HB) synthesis intermediates.

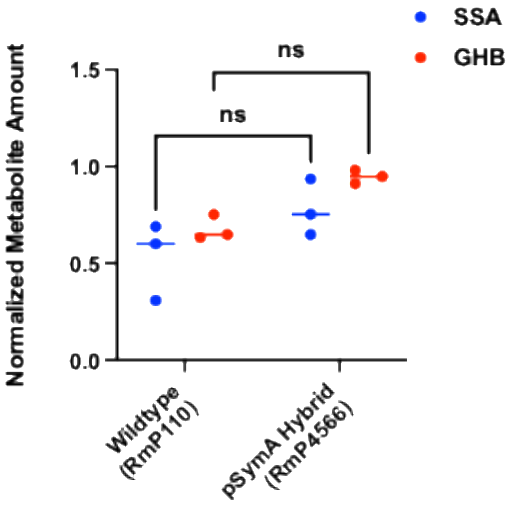

Supplemental Figure S17. Quantification of gamma-hydroxybutyrate and succinate-semialdehyde levels in *Medicago truncatula* nodules colonized by wildtype and HM006-pSymA hybrid strains. The quantity of the two metabolites is normalized to the amount detected in *Medicago sativa* nodules colonized by the wildtype (RmP110) strain **(Figure 5C).**

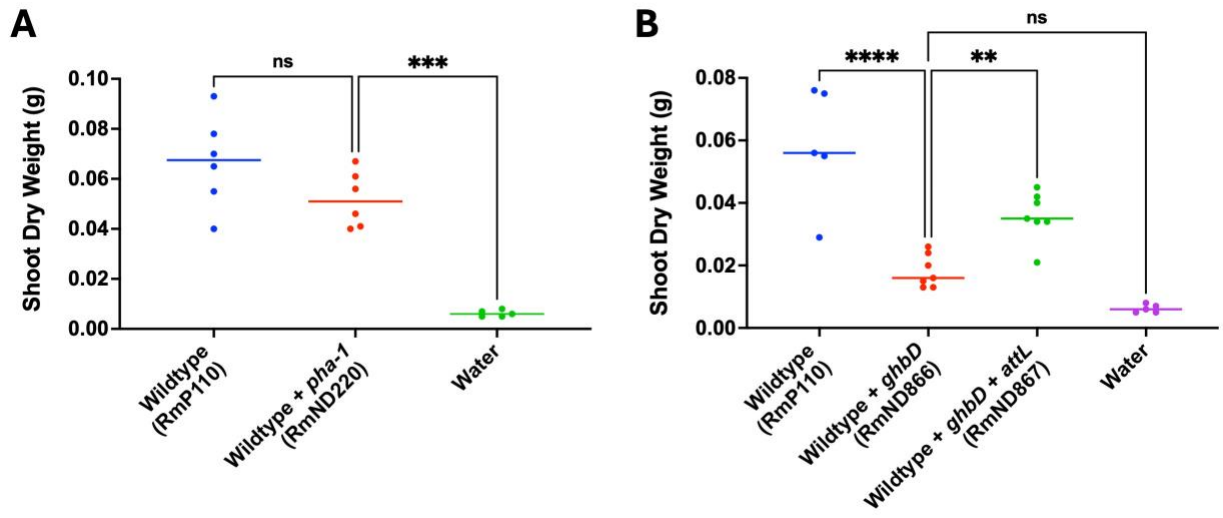

Supplemental Figure S18. Inclusion of *pha-1* to wildtype does not reduce shoot dry weight production by *Medicago truncatula* while inclusion of *ghbD* alone does, with the reduction in shoot dry weight alleviated through addition of *attL*. Quantitation of shoot dry weight accumulation by *M. truncatula* inoculated with **(A)** wildtype RmP110, wildtype with *pha-1*, and water or (B) with wildtype RmP110, wildtype with *ghbD*, wildtype with *ghbD* and *attL*, or water.

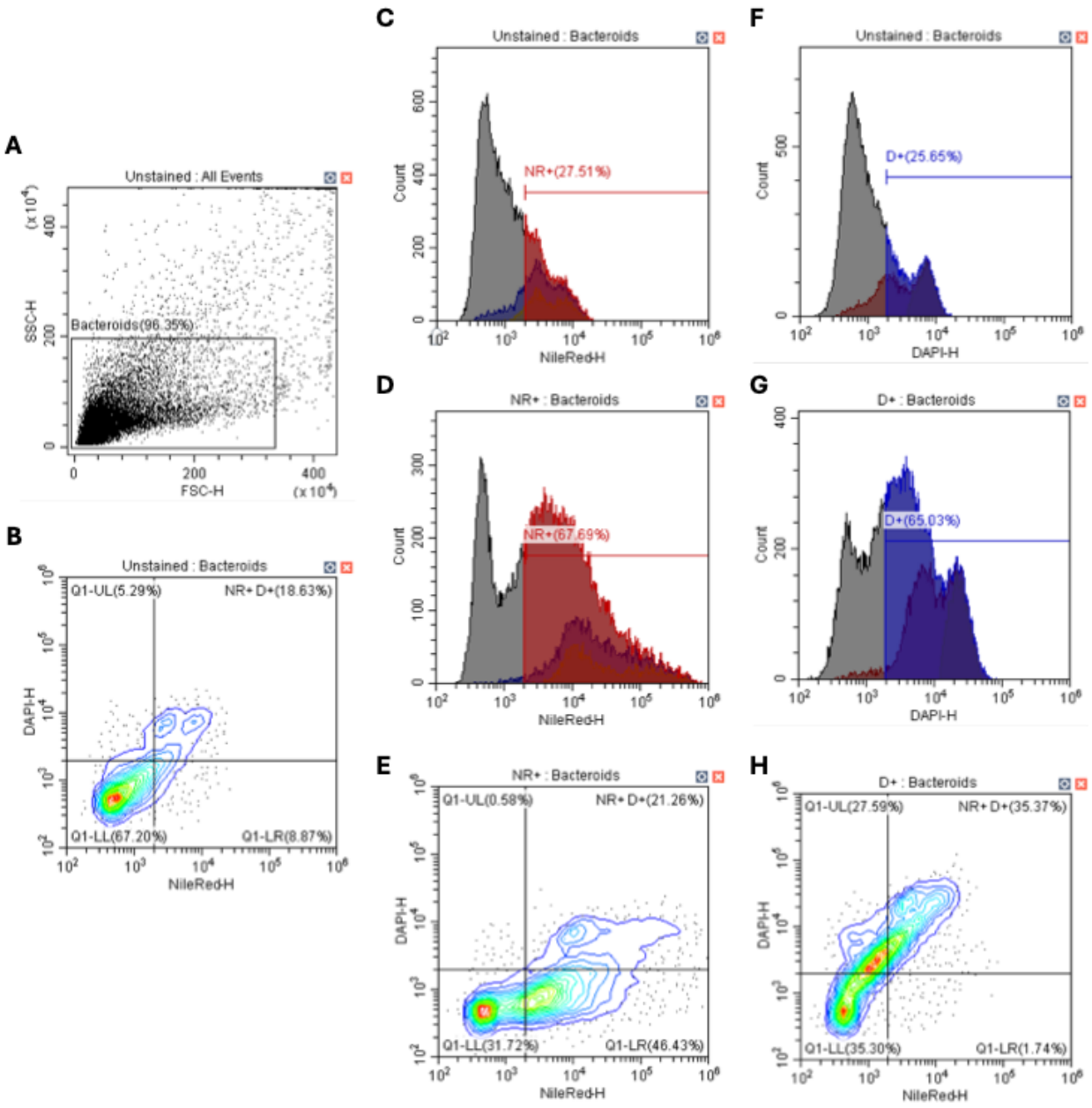

Supplemental Figure S19. Defining gating schemes and Nile Red and DAPI parameters for quantitation of PHA production by bacteroids via flow cytometry. (A) All events as depicted by side-scatter height versus forward-scatter height. “Bacteroids” were isolated events that excluded events too large to be deemed bacteroids, such as plant debris. All graphs (B-H) depict events within this gate. **(B)** Topographical plot depicting DAPI height versus Nile Red height of unstained “Bacteroids”. Used as the first passage for defining negative/positive

parameters of both DAPI and Nile Red. **(C and D)** Histograms depicting unstained negative (C) and Nile Red stained positive (D) controls. Both graphs were used to define Nile Red positive parameters. **(F and G)** Histograms depicting unstained negative (C) and DAPI stained positive (D) controls. Both graphs were used to define DAPI positive parameters. **(E and H)** Topographical plots depicting DAPI height versus Nile Red height of Nile Red only stained bacteroids (E) and DAPI only stained bacteroids. Used as the second passage for defining negative/positive parameters of both DAPI and Nile Red.

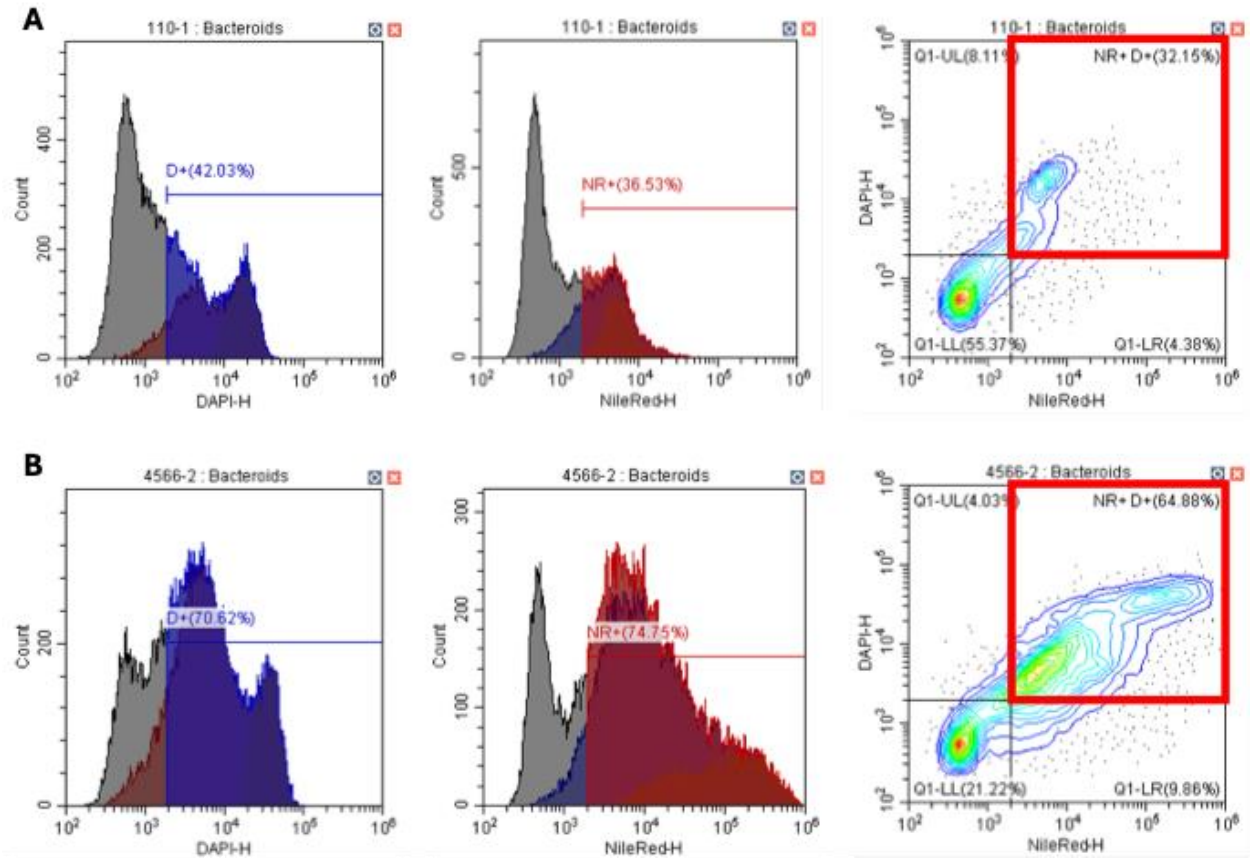

Supplemental Figure S20. Examples of negative and positive PHA producing bacteroids and their corresponding DAPI and Nile Red histograms and topographical plots. (A) Example data set of Rm1021 bacteroids that are unable to produce PHA during symbiosis. 32.15% of "Bacteroids" events are accounted for as DAPI positive and Nile Red positive (within red box). Within this 32.15% of events the mean Nile Red height was reported. **(B)** Example data set of RmP4566 (HM006 pSymA hybrid) bacteroids that produce PHA during symbiosis. 64.88% of "Bacteroids" events are accounted for as DAPI positive and Nile Red positive (within red box). Within this 64.88% of events the mean Nile Red height was reported.

Supplementary Methods

Microbial growth conditions

Bacterial strains and plasmids used in this work are listed in **S1**. *Escherichia coli* strains were grown at 37°C on LB (10 g L^{-1} tryptone, 10 g L^{-1} yeast extract, and 5 g L^{-1} NaCl). *Sinorhizobium meliloti* strains were grown at 30°C on LBmc (LB including 2.5 mM $MgSO_4$ and 2.5 mM $CaCl_2$). The following concentrations of antibiotics were used when working with *E. coli*: ampicillin (Amp) 100 µg mL^{-1}, chloramphenicol (Cm) 5 µg mL^{-1}, gentamycin (Gm) 20 µg mL^{-1}, kanamycin (Km) 25 µg mL^{-1}, rifampicin 25 µg mL^{-1}, spectinomycin (Sp) 50 µg mL^{-1}, and tetracycline (Tc) 5 µg mL^{-1}. A concentration of 40 µg mL^{-1} of 5-bromo-4-chloro-3-indolyl-beta-D-galactopyranoside (X-gal) was used when blue and white screening via *lacZ*. A concentration of 2.5 mM protocatechuate (PCA) was used for induction of FLP recombinase plasmids. When working with *S. meliloti* the following concentrations of antibiotics were used: gentamycin (Gm) 60 µg mL^{-1}, neomycin (Nm) 200 µg mL^{-1}, spectinomycin (Sp) 100 µg mL^{-1}, streptomycin (Sm) 200 µg mL^{-1}, and tetracycline (Tc) 5 µg mL^{-1}. *Saccharomyces cerevisiae* was grown at 30 °C using yeast extract peptone dextrose (YPD) complex media and synthetic complete (SC) defined media lacking histidine (12). Both types of yeast media were supplemented with 40 mg L^{-1} adenine hemisulfate.

Genetic manipulations

Conjugation

Plasmids housed within *E. coli* were routinely transferred into *S. meliloti* by conjugation via triparental mating between donor, helper (MT616), and recipient (13). In brief, overnight cultures of each strain were combined and spotted onto an LBmc mating plate and incubated overnight at 30°C. When using landing pads containing pTH2505 as the recipient strain, a final concentration of 2.5 mM protocatechuate was included in the mating plate. Controls of recipient only and donor with helper were also spotted. The following day mating spots were scraped into 1 mL of saline, diluted to 10^{-1} and 10^{-2}, then plated on the appropriate antibiotics and incubated for two nights at 30°C. When necessary to capture excised regions, conjugation via quadparental mating was used to transfer the plasmid of interest from *S. meliloti* into *E. coli*. In these instances, double *FRT* site integrants acted as the donor strain, with pTH1944 and MT616 as helper strains, and M859 as the recipient strain. *E. coli* transconjugants were selected for on LB with rifampicin and the appropriate antibiotic and incubated for one night at 37°C.

Transduction

Integrated plasmid constructs were moved between *S. meliloti* strains by transduction using the Φ M12 bacteriophage (2). Lysates were created of landing pad strains with integrated plasmid constructs by adding 100 µL of RmP110 lysate (infected by Φ M12 bacteriophage) to liquid cultures with an optical density of 0.4. Infection was allowed to occur overnight and if successful, resulted in a clear culture the following day. To kill any residual cells, 200 µL of chloroform was added to the lysate and allowed to incubate for two hours. To begin infection of the recipient strain, 500 µL of 1:25 diluted lysate was added to 500 µL of dense overnight culture of the recipient strain. This mixture was allowed to incubate for 20 minutes at 30°C. The mixture was washed twice with ½ LB and resuspended in 500 µL ½ LB. 200 µL of the mixture was plated onto ½ LB with the appropriate antibiotic. Lysate-only and recipient-only controls were also plated.

Creation of hybrid strains

Hybrid strains were constructed by conjugation of megaplasmids into *S. meliloti* plasmid-cured backgrounds (Rm5000 ΔpSymA (RmP4246), Rm5000 ΔpSymAB (RmP4275) and RmP110 ΔpSymA (RmP4247). Rm5000 ΔpSymAB was constructed from RmP4246 constructed as previously described by transferring essential genes from pSymB to the chromosome (14). Transfer of *S. meliloti* megaplasmids was promoted through *rctB*-mediated transfer by biparental mating (15). *S. medicae* plasmids were performed by *oriT*-mediated conjugation using triparental mating as described above. To enable this, suicide plasmids bearing *oriT* and antibiotic resistance markers were introduced to *S. medicae* 419 pSymA (pTH3275) and pSymB (pTH3331) to generate donor strains RP4355 and RmP4451. Transfer of plasmids to plasmid-cured recipients was selected by growth on M9 minimal medium with trigonelline as a sole carbon source to select for pSymA and succinate as a sole carbon source to select for pSymB. For pSymB-only hybrids, a near-isogenic pSymA was restored to the Rm5000 ΔpSymAB background after hybrid pSymB transfer by a second *rctB*-mediated conjugation from RmP110. Resulting hybrids were verified by genome resequencing.

Construction of deletions

Deletions were made using FLP-*FRT* recombination (9). This approach relies on the introduction of a flippase to initiate the recombination of separate *FRT* sites flanking the region to be excised. This recombination event results in the excision of the flanked region while leaving behind an *FRT* site. Integration of plasmids bearing *FRT* sites (pTH1937, pTH3291,

pNDGG014, and pNDGG015) into the pSymA of RmP4566 occurred via single-crossover homologous recombination. Introduction of these *FRT*- bearing plasmids, and eventually a flippase encoding plasmid (pTH1944), into *S. meliloti* occurred via triparental mating.

Plasmid construction

All primer sequences used to amplify homologous flanking regions are listed in **Supplemental Table S3**. Primers included tags containing an appropriate restriction site for ligation into a corresponding vector (BglII/PstI for pTH3291; KpnI/HindIII for pTH1937). After amplification using RmP4566 as template, inserts were verified via gel electrophoresis. After verification, amplicons were cleaned using a Qiagen PCR purification kit and quantified via Nanodrop. Inserts then underwent appropriate double restriction digest protocols. They were then combined with an appropriate vector (previously digested) in a ligation reaction with T4 ligase (insert and vector combinations can be found in **Supplemental Tables S1** and **S3**). To expedite the construction of plasmids we utilized Golden Gate Cloning. Tags for primers to be used in Golden Gate Cloning included a BsaI site and four bases homologous to the conjoining destination. All primers used to amplify homologous flanking regions are listed in **Supplemental Table S3**. After amplification using RmP4566 as template, inserts were verified via gel electrophoresis. After verification, amplicons were cleaned using a Qiagen PCR purification kit and quantified via Nanodrop. Inserts could then be used in a BsaI Golden Gate Cloning reaction with pNDGG014 or pNDGG015. When using pNDGG014 and pNDGG015, a separate plasmid containing an *FRT* site (FRT_EF) had to be added to the Golden Gate Cloning reaction. Putative plasmids were introduced into competent DH5-Alpha *E. coli* cells through heat shock transformation. Cells were then selected on the appropriate antibiotic (pTH3291 and pNDGG014 Gm^R; pTH1937 and pNDGG015 Km^R). Blue and white screening with *lacZ* was also utilized when using pNDGG014 or pNDGG015 as vector backbones. Putative colonies underwent restriction digest to verify correct assembly. A complete list of assembled plasmids can be found in **Supplemental Table S1**.

FLP/FRT recombination

After plasmid constructs were verified, they were then introduced individually to the genome of interest via conjugation by triparental mating (integration strategy can be found in **Supplemental Table S2**). If possible, *FRT* sites were first introduced between two bordering regions to be deleted. This allowed for one *FRT* site integration to be used for the creation of two separate double *FRT* site integrations. Transconjugants were selected for on Sm and either

Gm (pTH3291/pNDGG014) or Nm (pTH1937/pNDGG015). Putative colonies underwent PCR to verify plasmids integrated into the correct location. Primers were based in the genome (**Supplemental Table S4**) and in the plasmid backbone (**Supplemental Table S5**), amplifying across the junction. Primer pairings can be found in **Supplemental Table S6**.
The same workflow to create single *FRT* site integrations was used to create second *FRT* site integrations (refer to **Supplemental Table S2** for integration strategy). Transconjugants were selected for on Sm, Gm, and Nm. Putative colonies were verified via PCR in the same manner as single *FRT* site integrations. The presence of initial integrating plasmid was also screened for. Primer pairings can be found in **Supplemental Table S6**.
To initiate the recombination of *FRT* sites, and thus the excision of the flanked region, pTH1944 (FLP) was introduced to double *FRT* site integrants via triparental mating. Transconjugants were selected for on Sm and Tc (frequency of recombination seemed to occur at a higher rate when not using the remaining antibiotic as a measure of selection).

Verification of deletions
Colonies were then screened for either Gm^R Nm^S or Gm^S Nm^R depending on the location of *FRT* sites relative to the antibiotic resistance cassette housed within the vector backbone of the integrated flanking plasmids. Colonies showing the correct resistance and sensitivity pattern were then viewed as potentially having undergone successful *FRT* site recombination. These colonies were then verified to have had their *FRT* site flanked region excised via PCR. Primers were based in the backbone of the remaining integrated vector and in the genome of the other flanking region. The resulting amplification would span the junction between the two flanking regions, which was otherwise not possible if the region was still present. Primers and pairing used for deletion verification can be found in **Supplemental Table S7**.

Generation of gain-of-function constructs and strains
Strains made by yeast recombineering
ctrl-1 (R14), *pha-1* (R15), and *ctrl-2* (R16) were introduced individually into RmP110. Plasmid constructs containing *ctrl-1* (pNDMS119), *pha-1* (pNDMS120), and *ctrl-2* (pNDMS121) were assembled by yeast recombineering (a method of cloning that allows for several fragments of DNA to be assembled in one step) into the Sp^R BAC/YAC (bacterial/yeast artificial chromosome) multi-host shuttle vector pTH3369 via PacI. The method followed is detailed in Geddes et al, 2021. Fragments were amplified from RmP4566 template using Q5 High Fidelity DNA Polymerase (New England Biolabs) (primers for fragments used in assembly are listed in

Supplemental Table S8). Primers were based approximately 40 bp into adjacent fragments and/or vector backbones in order to adhere to one another during assembly. Linearized pTH3369 (via PacI) and fragments were transformed into *S. cerevisiae* VL6-48 following methods described in Gietz and Schiestl (12). Transformants were selected for on SC-His minimal media (i.e. histidine prototrophy). Newly assembled plasmids were isolated from *S. cerevisiae* using methods described in Brunwell et al. (16) and verified by PCR. Primers were based on either side of conjoining fragments, amplifying across the resulting junctions (primers used for verification of plasmids assembled by yeast recombineering are listed in **Supplemental Table S9**). Verified assemblies were then transformed by electroporation into Lucigen TransforMax EPI300 *E. coli.* Following high copy number induction by L-arabinose, plasmids were extracted from EPI300 and verified through restriction digest patterns. Plasmid sequences were verified by nanopore sequencing (Plasmidsaurus). After verification, plasmids were transformed into DH5-Alpha *E. coli*. This transformation allowed for the assembly to be introduced into the landing pad strain RmP4657 by triparental mating and integrated into the genome via FLP-*FRT* recombination initiated by an inducible flippase in pTH2505 (*FRT* site located in *manB*) (17). This integration allowed *ctrl-1* (RmND190), *pha-1* (RmND191), and *ctrl-2* (RmND192) to be transduced into RmP110 resulting in RmND219, RmND220, and RmND221, respectively. All strains and plasmids are listed in **Supplemental Table S1**.

Strains made by capturing excised region

R8 was also introduced individually into RmP110. When creating a deletion using FLP-*FRT* recombination, two *FRT* sites recombine in a manner that creates a “hybrid” *FRT* site containing one half of each site (occurs when both *FRT* sites are in same orientation). Due to this phenomenon, one complete *FRT* site is reconstituted within the genome, linking the genome back together while the region in between *FRT* sites is excised. A second *FRT* site is reconstituted in a manner that links the excised region into a circularized plasmid. Through quadriparental mating, the circularized plasmid comprised of the excised region could be “captured” or transferred into a M859 recipient strain. Double *FRT* site integrant RmND097 (R8) was used as a donor strain within the quadriparental mating. After the plasmid was captured, it was introduced into the landing pad strain RmP4657 by triparental mating and integrated into the genome via FLP-*FRT* recombination (17). This integration allowed *att* (RmND428) to be transduced into RmP110 resulting in RmND465. All strains and plasmids are listed in **Supplemental Table S1**.

To introduce *att* in combination with *pha-1*, it was necessary to introduce pNDMS041 (*att*) into landing pad strain RmP4253 (*FRT* site located in *hypRE*). Integration into RmP4253 allowed *att* (RmND468) to be transduced into RmND220 resulting in RmND522. All strains and plasmids are listed in **Supplemental Table S1**.

Genome resequencing

Genomic DNA was extracted from overnight liquid cultures grown in LBmc using the Qiagen *DNeasy UltraClean Microbial Kit* (Cat. No. 12224-250). DNA was randomly sheared into ~500bp fragments and the resulting fragments were used to create an Illumina library. This library was sequenced on an Illumina NovaSeq generating 150bp paired end reads. Custom reference sequences were created based on the publicly available genome sequenced from the replicons contained in each hybrid strain. Reads were aligned to the reference genome using BWA (18) and putative SNPs and small indels were called using samtools and mpileup (19). For projects with annotated genome reference, SNPs and small indel calls were annotated using SnpEff (20).Putative structural variants were called using a combination of BreakDancer (21), Pindel (22) and CNVnator (23). A summary of genome resequencing data is included in **Supplementary Table S11.**

RNA sequencing

Bacteroids were isolated from nodules collected from alfalfa 42 days post-inoculation. Nodules were picked directly onto dry ice, collected into 1.5 mL screw cap tubes, weighed, flash frozen via liquid nitrogen, and stored at -80 °C. Two volumes of bacteroid isolation buffer (1 M KH_2PO_4, 1 M K_2HPO_4, 300 mM sucrose, and 2 mM $MgCl_2$) was added to sample tubes (ex. 200 µL added to 100 mg nodules). After nodules were macerated, 200 µL of homogenized lysate was added to 400 µL RNAprotect (Qiagen cat. no. 76506) and vortexed. 300 µL of the mixture was saved and stored at -80 °C. The remaining 300 µL was centrifuged for 10 minutes at 5000 x *g* to pellet bacteroids and residual plant tissue. After the supernatant was removed, the pellet was resuspended in 700 µL of RLT with β-Mercaptoethanol. The mixture was then transferred to a Lysing Matrix B tube (MP Biomedicals REF: 6911100) and centrifuged. The remaining steps for RNA isolation followed from step two in the protocol for the Qiagen *RNeasy® Plus Mini Kit* and continued to completion. After extraction, RNA underwent DNase treatment following methods described in *RNAprotect® Bacteria Reagent Handbook: Appendix B: Optional On-Column DNase Digestion Using the RNase-Free DNase Set.* DNA contamination and RNA concentration was measured using the Qubit™ dsDNA HS Assay Kit (REF: Q32851) and

Qubit™ RNA BR Assay Kit (REF: Q10210), respectively. RNA quality was assessed using an Agilent TapeStation 4150 with RNA ScreenTape (Part No. 5067-5576).
RNA libraries were prepared using Illuminas Ribo-Zero rRNA Removal Kit (Bacteria) and the TruSeq Stranded Total RNA HT sample prep kit following the protocol outlined by Illumina in their user guide: https://support.illumina.com/sequencing/sequencing_kits/truseq-stranded-total-rna.html, and with the following conditions: total RNA starting material of 100 ng per sample and 10 cycles of PCR for library amplification. The prepared libraries were quantified using KAPA Biosystems' next-generation sequencing library qPCR kit and run on a Roche LightCycler 480 real-time PCR instrument. Sequencing of the flowcell was performed on the Illumina NovaSeq sequencer using NovaSeq XP V1.5 reagent kits, S4 flowcell, following a 2x151 indexed run recipe.
Raw fastq file reads were filtered and trimmed using the JGI QC pipeline resulting in the filtered fastq file (*.filter-RNA.gz files). Using BBDuk (24), raw reads were evaluated for artifact sequence by kmer matching (kmer=25), allowing 1 mismatch, and detected artifacts were trimmed from the 3' end of the reads. RNA spike-in reads, PhiX reads and reads containing any Ns were removed. Quality trimming was performed using the phred trimming method set at Q6. Finally, following trimming, reads under the length threshold were removed (minimum length 25 bases or 1/3 of the original read length - whichever is longer).Filtered reads from each library were aligned to the reference genome using HISAT2 version 2.2.1 (25) (BAMs/ directory). Strand-specific coverage bigWig files (fwd and rev) were generated using deepTools v3.1 (26) (bigWigs/ directory). featureCounts (27) was used to generate the raw gene counts (counts.txt) file using gff3 annotations, which were normalized to transcripts per million (TPM).

Isolation of GhbD

pNDMS331 was subcultured to an O.D. of 0.05 in 500 mL of autoinducing media (*Formedium #AIMSB0210*) with ampicillin. The culture was shaken at 250 rpm for 28 hours at 30°C, after which it was centrifuged for 15 minutes at 4000 g. The remaining cell pellet was resuspended in buffer (300 mM NaCl, 50 mM Na_3PO_4, 5 mM imidazole), sonicated, and centrifuged for 5 minutes at 14,000 g. The resulting supernatant was filtered through a 0.22 µm filter in preparation for sample purification using an ÄKTA go™ protein purification system by Cytiva. Buffers and run parameters were compatible with the column used for purification (*Bio-Rad #12009285*). Following purification, the sample underwent a buffer exchange using Zeba™ Spin Desalting Columns (*ThermoFischer Scientific #89882*). This introduced the protein to a buffer more suitable for downstream enzymatic assays (50 mM phosphate pH 7.4, 100 mM NaCl, and

10% glycerol). Various fractions were quantified using a Qubit® Protein Assay Kit (*ThermoFischer Scientific #Q33211*) and verified on precast polyacrylamide gels (*Bio-Rad #4561105*). An accompanying polyacrylamide gel image can be found in **Supplemental Figure S13**.

Metabolic Modelling

Flux balance analysis (FBA) was performed using a previously published genome-scale metabolic model representing the integrated metabolism of a *Sinorhizobium meliloti* nodulated *Medicago truncatula* plant, termed ViNE (32). Model manipulations and Flux Balance Analysis (FBA) were performed in MATLAB R2019B (mathworks.com) using the SBMLToolbox version 4.1.0 (33), libSBML version 5.13.0 (34), the iLOG CPLEX Studio 12.9.0 solver (ibm.com), and scripts from the COBRA Toolbox commit 492213a (35). Code to repeat the analysis is provided as File S1, while a copy of ViNE is provided as File S2.

ViNE does not include succinate semialdehyde (SSA) in the bacteroid component of the model. Therefore, to simulate the GhbD-mediated conversion of SSA to gamma-hydroxybutyrate (GHB), which would result in less conversion of SSA to succinic acid (SA), we added the following sink reaction to the zone III nitrogen-fixing bacteriods ViNE: *succinic acid + NADH + H^+ -> NAD^+*. This reaction would therefore simulate the decrease in succinate available to central metabolism due to the diversion of SSA to GHB (instead of succinate) and the associated reductant cost. To explore whether the observed metabolic effects were driven more by the diversion of carbon away from central metabolism or the reductant cost, we alternatively added one of the following two sink reactions to the zone III nitrogen-fixing bacteroids: (i) *succinic acid -> nothing* (to simulate the carbon cost; or (ii) *NADH + H^+ -> NAD^+* (to simulate the reductant cost). The effect of the sink reactions on growth rate and overall metabolism were then simulated by forcing flux through the sink reaction by adjusting the lower bound, and optimizing plant growth rate with the *optimizeCbModel* function of the COBRA Toolbox.

Supplementary References

1. H. M. Meade, S. R. Long, G. B. Ruvkun, S. E. Brown, F. M. Ausubel, Physical and genetic characterization of symbiotic and auxotrophic mutants of Rhizobium meliloti induced by transposon Tn5 mutagenesis. *J Bacteriol* **149**, 114–122 (1982).

2. T. M. Finan, *et al.*, General transduction in Rhizobium meliloti. *Journal of Bacteriology* **159**, 120–124 (1984).

3. Z.-C. Yuan, R. Zaheer, T. M. Finan, Regulation and Properties of PstSCAB, a High-Affinity, High-Velocity Phosphate Transport System of *Sinorhizobium Meliloti*. *Journal of Bacteriology* **188**, 1089–1102 (2006).

4. M. Nelson, J. Guhlin, B. Epstein, P. Tiffin, M. J. Sadowsky, The complete replicons of 16 Ensifer meliloti strains offer insights into intra- and inter-replicon gene transfer, transposon-associated loci, and repeat elements. *Microb Genom* **4**, e000174 (2018).

5. W. Reeve, *et al.*, Complete genome sequence of the Medicago microsymbiont Ensifer (Sinorhizobium) medicae strain WSM419. *Stand Genomic Sci* **2**, 77–86 (2010).

6. L. M. Sather, *et al.*, A broadly distributed predicted helicase/nuclease confers phage resistance via abortive infection. *Cell Host Microbe* **31**, 343-355.e5 (2023).

7. B. A. Geddes, *et al.*, Minimal gene set from Sinorhizobium (Ensifer) meliloti pSymA required for efficient symbiosis with Medicago. *Proceedings of the National Academy of Sciences* **118** (2021).

8. H. P. Schweizer, Vectors to express foreign genes and techniques to monitor gene expression in Pseudomonads. *Curr Opin Biotechnol* **12**, 439–445 (2001).

9. B. Milunovic, G. C. diCenzo, R. A. Morton, T. M. Finan, Cell Growth Inhibition upon Deletion of Four Toxin-Antitoxin Loci from the Megaplasmids of Sinorhizobium meliloti. *J Bacteriol* **196**, 811–824 (2014).

10. C. L. M. Gilchrist, Y.-H. Chooi, clinker & clustermap.js: automatic generation of gene cluster comparison figures. *Bioinformatics* **37**, 2473–2475 (2021).

11. A. C. E. Darling, B. Mau, F. R. Blattner, N. T. Perna, Mauve: Multiple Alignment of Conserved Genomic Sequence With Rearrangements. *Genome Res* **14**, 1394–1403 (2004).

12. R. D. Gietz, R. H. Schiestl, High-efficiency yeast transformation using the LiAc/SS carrier DNA/PEG method. *Nature protocols* **2**, 31–34 (2007).

13. T. M. Finan, B. Kunkel, G. F. De Vos, E. R. Signer, Second symbiotic megaplasmid in Rhizobium meliloti carrying exopolysaccharide and thiamine synthesis genes. *J Bacteriol* **167**, 66–72 (1986).

14. G. C. diCenzo, A. M. MacLean, B. Milunovic, G. B. Golding, T. M. Finan, Examination of Prokaryotic Multipartite Genome Evolution through Experimental Genome Reduction. *PLOS Genetics* **10**, e1004742 (2014).

15. A. Checcucci, *et al.*, Creation and Characterization of a Genomically Hybrid Strain in the Nitrogen-Fixing Symbiotic Bacterium Sinorhizobium meliloti. *ACS Synth. Biol.* **7**, 2365–2378 (2018).

16. S. L. Brumwell, *et al.*, Designer Sinorhizobium meliloti strains and multi-functional vectors enable direct inter-kingdom DNA transfer. *PLoS One* **14**, e0206781 (2019).

17. B. A. Geddes, *et al.*, Minimal gene set from *Sinorhizobium (Ensifer) meliloti* pSymA required for efficient symbiosis with *Medicago*. *Proceedings of the National Academy of Sciences* **118**, e2018015118 (2021).

18. H. Li, R. Durbin, Fast and accurate short read alignment with Burrows–Wheeler transform. *Bioinformatics* **25**, 1754–1760 (2009).

19. H. Li, *et al.*, The Sequence Alignment/Map format and SAMtools. *Bioinformatics* **25**, 2078–2079 (2009).

20. P. Cingolani, *et al.*, A program for annotating and predicting the effects of single nucleotide polymorphisms, SnpEff: SNPs in the genome of Drosophila melanogaster strain w1118; iso-2; iso-3. *Fly* **6**, 80–92 (2012).

21. K. Chen, *et al.*, BreakDancer: an algorithm for high-resolution mapping of genomic structural variation. *Nat Methods* **6**, 677–681 (2009).

22. K. Ye, M. H. Schulz, Q. Long, R. Apweiler, Z. Ning, Pindel: a pattern growth approach to detect break points of large deletions and medium sized insertions from paired-end short reads. *Bioinformatics* **25**, 2865–2871 (2009).

23. A. Abyzov, A. E. Urban, M. Snyder, M. Gerstein, CNVnator: an approach to discover, genotype, and characterize typical and atypical CNVs from family and population genome sequencing. *Genome Res* **21**, 974–984 (2011).

24. BBMap. *SourceForge* (2023). Available at: https://sourceforge.net/projects/bbmap/ [Accessed 8 April 2024].

25. D. Kim, B. Langmead, S. L. Salzberg, HISAT: a fast spliced aligner with low memory requirements. *Nat Methods* **12**, 357–360 (2015).

26. F. Ramírez, F. Dündar, S. Diehl, B. A. Grüning, T. Manke, deepTools: a flexible platform for exploring deep-sequencing data. *Nucleic Acids Res* **42**, W187–W191 (2014).

27. Y. Liao, G. K. Smyth, W. Shi, featureCounts: an efficient general purpose program for assigning sequence reads to genomic features. *Bioinformatics* **30**, 923–930 (2014).

28. Bentham, A.R., Youles, M., Mendel, M.N., Varden, F.A., De la Concepcion, J.C., and Banfield, M.J. 2021. pOPIN-GG: A Resource for Modular Assembly in Protein Expression Vectors. *bioRxiv.* 201.08.10.455798

29. Geddes, B.A., Williamson, R., Schumacher, J., Ardi, A., Levin, G., Červenka, E., Huang, R., and DiCenzo, G.C. 2025. BEVA2.0: Modular Assembly of Golden Gate-Compatible

Vectors with Expanded Utility for Genetic Engineering. *Canadian Journal of Microbiology.* **71**, 1-13.

30. Geddes, B.A., Mendoza-Suárez, M.A., and Poole, P.S. 2019. A Bacterial Expression Vector Archive (BEVA) for Flexible Modular Assembly of Golden Gate-Compatible Vectors. *Frontiers in Microbiology*. 9. 2018.03345.

31. Ardi, A. 2023. Improving Symbiotic Nitrogen Fixation in *Sinorhizobium* (*Ensifer*) *meliloti* by Utilizing Synthetic Biology Approaches to Manipulate Key Regulatory Genes. *ProQuest Dissertations and Theses*. M.S., North Dakota State University.

32. diCenzo GC, Tesi M, Pfau T, Mengoni A, Fondi M. 2020. Genome-scale metabolic reconstruction of the symbiosis between a leguminous plant and a nitrogen-fixing bacterium. Nat Commun 11:2574.

33. Keating SM, Bornstein BJ, Finney A, Hucka M. 2006. SBMLToolbox: an SBML toolbox for MATLAB users. Bioinformatics 22:1275–1277.

34. Bornstein BJ, Keating SM, Jouraku A, Hucka M. 2008. LibSBML: an API library for SBML. Bioinformatics 24:880–881.

35. Heirendt L, Arreckx S, Pfau T, Mendoza SN, Richelle A, Heinken A, Haraldsdóttir HS, Wachowiak J, Keating SM, Vlasov V, Magnusdóttir S, Ng CY, Preciat G, Žagare A, Chan SHJ, Aurich MK, Clancy CM, Modamio J, Sauls JT, Noronha A, Bordbar A, Cousins B, El Assal DC, Valcarcel LV, Apaolaza I, Ghaderi S, Ahookhosh M, Ben Guebila M, Kostromins A, Sompairac N, Le HM, Ma D, Sun Y, Wang L, Yurkovich JT, Oliveira MAP, Vuong PT, El Assal LP, Kuperstein I, Zinovyev A, Hinton HS, Bryant WA, Aragón Artacho FJ, Planes FJ, Stalidzans E, Maass A, Vempala S, Hucka M, Saunders MA, Maranas CD, Lewis NE, Sauter T, Palsson BØ, Thiele I, Fleming RMT. 2019. Creation and analysis of biochemical constraint-based models using the COBRA Toolbox v.3.0. Nat Protoc 14:639–702.